# Phospholipid order in gel- and fluid-phase cell-size liposomes measured by digitized video fluorescence polarization microscopy

Kathryn Florine-Casteel
Curriculum in Toxicology and Department of Cell Biology and Anatomy, University of North Carolina at Chapel Hill, Chapel Hill, North Carolina 27599 USA

ABSTRACT Low-light digitized video fluorescence microscopy has been utilized to measure the steady-state polarized fluorescence from the membrane probe diphenylhexatriene (DPH) and its cationic and phosphatidylcholine derivatives 1-(4-trimethylammoniumphenyl)-6-phenyl-1,3,5-hexatriene (TMA-DPH) and 2-[3-(diphenylhexatrienyl)propanoyl]-3-palmitoyl-L-$\alpha$-phosphatidylcholine (DPH-PC), respectively, in cell-size (10–70 $\mu$m) unilamellar vesicles composed of gel- or fluid-phase phospholipid. Using an inverted microscope with epi-illumination optics and an intensified silicon intensified target camera interfaced to a minicomputer, fluorescence images of single vesicles were obtained at emission polarizer orientations of 0°, 45°, 90°, and 135° relative to the excitation light polarization direction. Fluorescence intensity ratios $F_{90°}/F_{0°}$ ($=F_{\perp}/F_{\parallel}$) and $F_{135°}/F_{45°}$ were calculated on a pixel-by-pixel basis from digitized image pairs. Theoretical expressions were derived for collected polarized fluorescence as a function of position on the membrane surface as well as the degree of lipid order, in terms of the fluorophore's maximum angular motional freedom in the bilayer ($\equiv\theta_{max}$), using a modification of the method of D. Axelrod (1979. *Biophys. J.* 26:557–574) together with the "wobbling-in-a-cone" model of probe rotational diffusion. Comparison of experimental polarization ratios with theoretical ratios yielded the following results. In gel-phase dipalmitoylphosphatidylcholine, the data for all three probes correspond to a model in which the cone angle $\theta_{max} = 17 \pm 2°$ and there exists a collective tilt of the phospholipid acyl chains of 30° relative to the bilayer normal. In addition, ~5% of DPH and TMA-DPH molecules are aligned parallel to the plane of the bilayer. In fluid-phase palmitoyloleoylphosphatidylcholine, the data are well fit by models in which $\theta_{max} = 60 \pm 2°$ for DPH and DPH-PC and $32 \pm 4°$ for TMA-DPH, with ~20% of DPH molecules and 10% of TMA-DPH molecules aligned parallel to the bilayer plane, and a net phospholipid tilt at or near the headgroup region of ~30°. The results demonstrate that lipid order can be measured with a spatial resolution of ~1 $\mu m^2$ in cell-size vesicles even with high aperture observation through a microscope.

## INTRODUCTION

The relationship between plasma membrane structure and function is poorly understood. There is growing evidence to support the idea that a variety of cellular events associated with the plasma membrane, such as transmembrane signal transduction, transport phenomena, and membrane fusion, may involve local changes in the physical state of the membrane, for example the formation of gel-phase lipid domains (see Grant, 1983, and Jain, 1983, for recent reviews).

One of the most widely used methods of measuring membrane lipid order, often termed "fluidity", has been fluorescence polarization spectroscopy (see, for example, Lentz, 1988). However, spectroscopic methods in general yield information on average probe behavior in a population of vesicles or cells. If there exist cell processes which are mediated by changes in plasma membrane lipid order, those changes are likely to be very localized. Therefore, the ability to measure lipid order with subcellular resolution would be of great value. The objective of this study was to test the feasibility of such measurements using steady-state fluorescence polarization microscopy combined with digital image processing. Formulae relating the observed orientation-dependent fluorescence polarization to the degree of lipid order were developed, and then applied to a model system of cell-size unilamellar phospholipid vesicles labeled with diphenylhexatriene (DPH)[1] probes.

The major difficulties associated with microscopic fluorescence polarization measurements are the depolarizing effect of the microscope optics (von Sengbusch and

Address correspondence to Dr. Kathryn Florine-Casteel, Department of Cell Biology and Anatomy, University of North Carolina at Chapel Hill, CB#7090, 202 Taylor Hall, Chapel Hill, NC 27599.

[1] *Abbreviations used in this paper:* DPH, 1,6-diphenyl-1,3,5-hexatriene; DPH-PC, 2-[3-(diphenylhexatrienyl)propanoyl]-3-palmitoyl-L-$\alpha$-phosphatidylcholine; DPPC, 1,2-dipalmitoyl-*sn*-glycero-3-phosphocholine; POPC, 1-palmitoyl-2-oleoyl-*sn*-glycero-3-phosphocholine, TMA-DPH, 1-(4-trimethylammoniumphenyl)-6-phenyl-1,3,5-hexatriene.

Thaer, 1973) and, for membrane surface probes, the orientation dependence of the observed fluorescence intensities. These issues were addressed in a study by Axelrod (1979) in which the orientation of long-chain carbocyanine dyes in erythrocyte ghosts was determined using steady-state fluorescence polarization microscopy. Theoretical expressions were derived for polarized fluorescence intensity as a function of location on the membrane surface, based on a model for probe orientation and dynamics in the bilayer. Experimental polarization ratios were measured at three surface locations, using an image plane diaphragm, and compared with the corresponding theoretical ratios to determine the most plausible probe orientation in the membrane.

The study presented here utilizes fundamentally the approach of Axelrod (1979), except that it employs a probe type which is sensitive to lipid acyl chain order and an imaging system that yields quantitative information over the entire membrane surface. Using a probe excited-state orientation distribution function based on the "wobbling-in-a-cone" model of rotational diffusion, theoretical expressions were obtained for polarized fluorescence intensity as a function of angular constraint of probe motion (in terms of a "cone angle") and position on the membrane surface. Fluorescence polarization ratio images were obtained for DPH, 1-(4-trimethylammoniumphenyl)-6-phenyl-1,3,5-hexatriene (TMA-DPH), and 2-[3-(diphenylhexatrienyl)propanoyl]-3-palmitoyl-L-$\alpha$-phosphatidylcholine (DPH-PC) in both gel-phase dipalmitoylphosphatidylcholine (DPPC) and fluid-phase palmitoyloleoylphosphatidylcholine (POPC) vesicles. The experimental results indicate that differences in lipid order can be resolved on the surface of a cell-size vesicle imaged through a microscope. Furthermore, comparison of experimental and theoretical polarization ratios yields results for probe location and degree of motional freedom that are in good agreement with those reported in the literature based on spectroscopic studies.

Preliminary results of this work were presented at the International Conference on Video Microscopy held at the University of North Carolina at Chapel Hill in June 1989.

## THEORY

### Microscopy vs. fluorometry

In a conventional steady-state fluorescence polarization experiment, a membrane suspension in a cuvette is illuminated with linearly polarized light and probe fluorescence is measured through an analyzing polarizer oriented parallel ($F_\parallel$) and also perpendicular ($F_\perp$) to the exciting light polarization direction. Fluorophore rotations occurring on the timescale of the excited-state lifetime will lead to depolarization of fluorescence, which is usually expressed in terms of the fluorescence anisotropy

$$r \equiv \frac{F_\parallel - F_\perp}{F_\parallel + 2F_\perp}. \quad (1)$$

The more disordered the membrane environment, the greater is the motional freedom of the fluorophore and hence the lower the observed anisotropy (i.e., $F_\perp/F_\parallel$ approaches unity). Single cell-size vesicles viewed through a microscope constitute a highly oriented rather than an isotropic sample. Consequently, the anisotropy (or equivalently $F_\perp/F_\parallel$) measured microscopically will vary not only with lipid order but also with position on the membrane surface. To interpret the data, the functional dependence of polarized fluorescence on lipid order as well as on surface location must be determined.

The factors which affect the fluorescence polarization observed in a microscope image are illustrated schematically in Figs. 1 and 2. The sphere in Fig. 1 represents a lipid vesicle on the microscope stage, focused at the $X_2 - X_3$ plane. For a probe molecule at an arbitrary location ($\rho$, $\gamma$) on the membrane surface, the observed polarized fluorescence will depend on the absorption dipole orientation relative to the exciting light polarization direction ($X_3$), as well as the change in probe orientation between absorption and emission of a photon. For example, DPH probe molecules in the vicinity of ($\rho$, $\gamma$) = (0°, 0°) in a rigid membrane environment (low $\theta_{max}$) would have a high probability of excitation, with fluorescence polarized predominantly in the $X_3$ direction. Another factor is the high numerical aperture of the objective lens, which causes mixing in of fluorescence from dipole moment components in the $X_1$ and $X_2$ directions in the recorded $F_\parallel$ image and, similarly, mixing in of $X_1$ and $X_3$ components in the $F_\perp$ image. Lastly, because the microscope images are two-dimensional projections of a three-dimensional object, the region of the membrane surface defined by each image pixel is dependent on pixel size and location. The measurement area for the vesicle perimeter region, in the focal plane, is illustrated in Fig. 2. In contrast, the center of the vesicle image will contain out-of-focus fluorescence contributions from both the upper and lower surfaces, in the vicinity of $\gamma = \pm 90°$ (Fig. 1, *left*).

### Model of probe motion

In deriving mathematical expressions for fluorescence polarization as a function of lipid order and membrane surface location, we must make use of a model for probe rotational diffusion during the excited-state lifetime. From the model we can obtain the probe excited-state

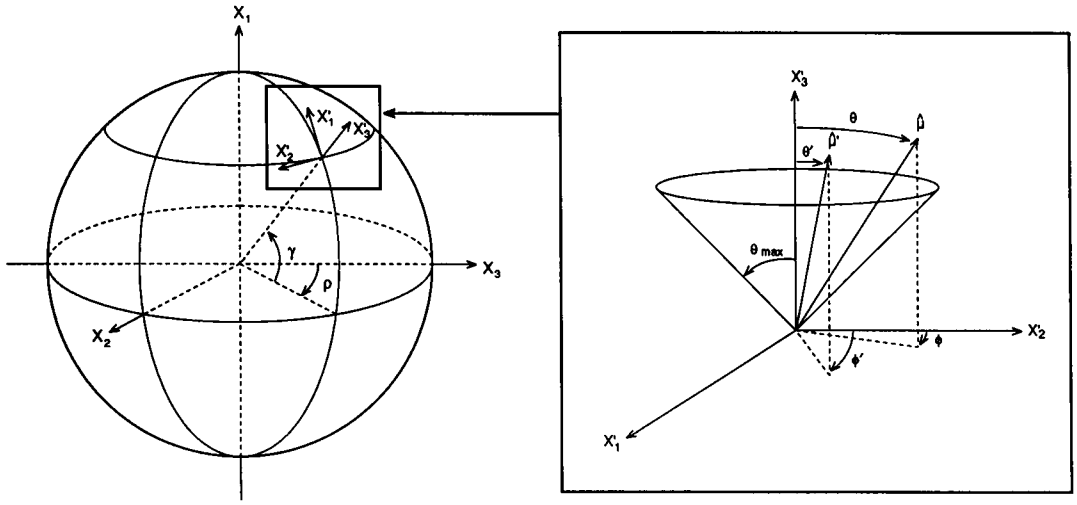


FIGURE 1 Definition of coordinates. In the laboratory (*unprimed*) frame, the $X_1$-axis is the optical axis of the microscope and the $X_2$- and $X_3$-axes define the focal plane. Incident excitation light reflected through the condenser/objective to the sample from the dichroic mirror below (not shown) is polarized in the $X_3$ direction. Emitted fluorescence is collected at 180° to the incident light propagation direction with a rotatable polarizer in the emission path whose orientation in the $X_2 - X_3$ plane can be varied from 0° to 360° with respect to the positive $X_3$-axis. The angles $\rho$ and $\gamma$ specify an arbitrary point on the spherical membrane surface. In the membrane (*primed*) frame, enlarged on the right, the $X'_3$-axis is normal to the surface. Parallel probe absorption and emission dipole moments are assumed; excitation occurs at dipole orientation $(\theta', \phi')$ at time $t'$ and emission occurs at $(\theta, \phi)$ at time $t(>t')$. The angle $\theta_{max}$ represents the maximum angular deviation of a dipole from the bilayer normal.

orientation distribution, which can then be used to determine the orientation-dependent polarized fluorescence.

A physically reasonable diffusion model for the rod-shaped fluorophores utilized in this study is the "wobbling-in-a-cone" model introduced by Kinosita and coworkers (1977), in which the probe wobbles unhindered in a cone of semiangle $\theta_{max}$ (Fig. 1, *right*). The cone angle $\theta_{max}$ is related to the orientational order parameter, $S$, by

$$S = \left(\frac{1}{2}\right)\cos\theta_{max}\,(1 + \cos\theta_{max}) \tag{2}$$

(Lipari and Szabo, 1980). In this model, the probability $p(\theta', \phi', t'|\theta, \phi, t)$ that a probe having orientation $(\theta', \phi')$ at time $t'$ will have orientation $(\theta, \phi)$ at a later time $t$ obeys the Smoluchowski equation for a potential of the form

$$V(\theta) = \begin{cases} 0 & \text{if } 0 \le \theta \le \theta_{max} \\ \infty & \text{if } \theta > \theta_{max} \end{cases}, \tag{3}$$

given by

$$\frac{\partial p(\theta', \phi', t'|\theta, \phi, t)}{\partial t} = D_w\left[\frac{1}{\sin\theta}\frac{\partial}{\partial\theta}\left(\sin\theta\frac{\partial}{\partial\theta}\right) + \frac{1}{\sin^2\theta}\frac{\partial^2}{\partial\phi^2}\right] \cdot p(\theta', \phi', t'|\theta, \phi, t) \tag{4}$$

in the region $0 \le \theta \le \theta_{max}$, where $D_w$ is the "wobbling" diffusion coefficient, subject to the delta-function initial condition

$$p(\theta', \phi', t'|\theta, \phi, t') = \delta(\cos\theta - \cos\theta')\delta(\phi - \phi') \tag{5}$$

and the boundary condition

$$\left.\frac{\partial p(\theta', \phi', t'|\theta, \phi, t)}{\partial\theta}\right|_{\theta=\theta_{max}} = 0. \tag{6}$$

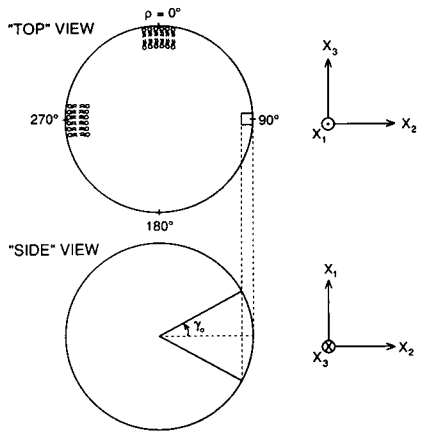


FIGURE 2 Observation area. For measurements in the $X_2 - X_3$ plane ($0° \le \rho \le 360°$, $\gamma = 0°$) at the vesicle edges, the actual range of $\gamma$ included in each pixel in the image is dependent on pixel size (illustrated by the square at $\rho = 90°$) and ranges from $-\gamma_0$ to $+\gamma_0$ where $\gamma_0 = \cos^{-1}[(r - x)/r]$, $x$ = pixel diameter, and $r$ = vesicle radius. Phospholipid orientation in the focal plane is partially illustrated in the "top" view, i.e., the view along the optical axis.

The (Green function) solution of Eq. 4 which satisfies Eqs. 5 and 6, found by the method of separation of variables, can be written as

$$p(\theta', \phi', t'|\theta, \phi, t) = \frac{1}{2\pi}\sum_{n=0}^{\infty}{}'\left[\frac{1}{N_n}P_n(\cos\theta')\,P_n(\cos\theta) + 2\sum_{m=1}^{n}{}'\frac{1}{N_n^m}(-1)^m\frac{(n-m)!}{(n+m)!} \cdot P_n^m(\cos\theta')\,P_n^m(\cos\theta)\cos m(\phi-\phi')\right] \cdot e^{-n(n+1)D_w(t-t')}, \quad (7)$$

where $P_n(\cos\theta)$ and $P_n^m(\cos\theta)$ are Legendre and associated Legendre functions, respectively. The notation $\Sigma'$ indicates summation over only those $n$ and $m$ for which $\partial P_n/\partial\theta|_{\theta=\theta_{max}} = 0$ and $\partial P_n^m/\partial\theta|_{\theta=\theta_{max}} = 0$, i.e., those $n$ and $m$ for which Eq. 6 is satisfied. $N_n$ and $N_n^m$ are normalization constants, given by

$$N_n = \int_0^{\theta_{max}}[P_n(\cos\theta)]^2\sin\theta\,d\theta \quad (8)$$

$$N_n^m = \int_0^{\theta_{max}}(-1)^m\frac{(n-m)!}{(n+m)!}[P_n^m(\cos\theta)]^2\sin\theta\,d\theta. \quad (9)$$

## Derivation of expressions for orientation-dependent fluorescence polarization

Once $p(\theta', \phi', t'|\theta, \phi, t)$ has been determined, the angular distribution of excited-state molecules over the spherical membrane surface, denoted by $f(\theta, \phi, \rho, \gamma, \theta_{max})$, can be obtained from the relation

$$f(\theta, \phi, \rho, \gamma, \theta_{max}) = \frac{1}{\tau}\int_{\theta'=0}^{\theta_{max}}\int_{\phi'=0}^{2\pi}\int_{(t-t')=0}^{\infty}x_3^2(\theta', \phi', \rho, \gamma) \cdot p(\theta', \phi', t'|\theta, \phi, t)\,e^{-(t-t')/\tau} \cdot \sin\theta'\,d\theta'\,d\phi'\,d(t-t'), \quad (10)$$

where $x_3(\theta', \phi', \rho, \gamma)$ is the component of a unit magnitude absorption dipole along the $X_3$-axis (the excitation light polarization direction) at the time of absorption ($t - t' = 0$, see Fig. 1) and $\tau$ is the probe excited-state lifetime. Transformed from the membrane to the laboratory frame, the components $x_i(\theta', \phi', \rho, \gamma)$ of an absorption dipole moment are

$$x_1 = \cos\gamma\sin\theta'\sin\phi' + \sin\gamma\cos\theta' \quad (11)$$

$$x_2 = \cos\rho\sin\theta'\cos\phi' - \sin\rho\,\sin\gamma\sin\theta'\sin\phi' + \sin\rho\cos\gamma\cos\theta' \quad (12)$$

$$x_3 = -\sin\rho\sin\theta'\cos\phi' - \cos\rho\sin\gamma\sin\theta'\sin\phi' + \cos\rho\cos\gamma\cos\theta'. \quad (13)$$

Substitution of Eqs. 7 and 13 into Eq. 10, followed by integration, yields

$$f(\theta, \phi, \rho, \gamma, \theta_{max}) = \sum_{\text{even}\,n=0}^{\infty}{}'\frac{P_n(\cos\theta)}{N_n[1 + n(n+1)D_w\tau]} \cdot \left[T_n\cos^2\gamma\cos^2\rho + \frac{1}{2}U_n(\sin^2\rho + \sin^2\gamma\cos^2\rho)\right] + \sum_{\text{even}\,n=2}^{\infty}{}' \cdot \frac{(n-2)!}{(n+2)!}\frac{P_n^2(\cos\theta)}{2N_n^2[1 + n(n+1)D_w\tau]} \cdot V_n[\cos 2\phi(\sin^2\rho - \sin^2\gamma\cos^2\rho) + \sin 2\phi\sin\gamma\sin 2\rho], \quad (14)$$

where $T_n$, $U_n$, and $V_n$ are functions of the cone angle $\theta_{max}$, defined as follows for $\theta'$ or $\theta$:

$$T_n \equiv \int_0^{\theta_{max}}P_n(\cos\theta')\cos^2\theta'\sin\theta'\,d\theta' \quad (15)$$

$$U_n \equiv \int_0^{\theta_{max}}P_n(\cos\theta')\sin^3\theta'\,d\theta' \quad (16)$$

$$V_n \equiv \int_0^{\theta_{max}}P_n^2(\cos\theta')\sin^3\theta'\,d\theta'. \quad (17)$$

Only the $m = 0$ and $m = 2$ terms survive the integration over $\phi'$. The use of only terms even in $n$ is required for invariance of $f$ under inversion of the symmetry axis (i.e., the cone axis), because probes may reside in either leaflet of the bilayer. Because of the boundary condition on $p(\theta', \phi', t'|\theta, \phi, t)$ (Eq. 6), the explicit form of $f(\theta, \phi, \rho, \gamma, \theta_{max})$ will vary with the value of $\theta_{max}$ for which it is evaluated.

The emission dipole orientation distribution function $f(\theta, \phi, \rho, \gamma, \theta_{max})$ can now be used to calculate fluorescence polarization. For an arbitrary orientation $\psi$ of the emission polarizer in the $X_2 - X_3$ plane, the normalized fluorescence intensity collected from the location $(\rho, \gamma)$ on the membrane surface is

$$F_\psi(\rho, \gamma, \theta_{max}) = \frac{1}{2\pi(1-\cos\theta_{max})}\int_{\theta=0}^{\theta_{max}}\int_{\phi=0}^{2\pi}f(\theta, \phi, \rho, \gamma, \theta_{max}) \cdot [K_a x_1^2 + (K_b\cos^2\psi + K_c\sin^2\psi)x_2^2 + (K_b\sin^2\psi + K_c\cos^2\psi)x_3^2 + 2(K_c - K_b) \cdot \sin\psi\cos\psi x_2x_3]\sin\theta\,d\theta\,d\phi \quad (18)$$

where $x_1$, $x_2$, and $x_3$ are the components of a unit magnitude emission dipole moment along the $X_1$-, $X_2$-, and $X_3$-axes, respectively, given by Eqs. 11–13 except with $\theta'$ and $\phi'$ replaced by $\theta$ and $\phi$. $K_a$, $K_b$, and $K_c$ are weighting factors that depend on the numerical aperture (NA) of the objective and the refractive index (n) of the medium in which the sample is embedded, expressed in

normalized form as

$$K_a = \frac{1}{6(1 - \cos\sigma_0)}(2 - 3\cos\sigma_0 + \cos^3\sigma_0) \quad (19)$$

$$K_b = \frac{1}{24(1 - \cos\sigma_0)}(1 - 3\cos\sigma_0 + 3\cos^2\sigma_0 - \cos^3\sigma_0) \quad (20)$$

$$K_c = \frac{1}{8(1 - \cos\sigma_0)}(5 - 3\cos\sigma_0 - \cos^2\sigma_0 - \cos^3\sigma_0), \quad (21)$$

where

$$\mathrm{NA} = \mathrm{n}\sin\sigma_0 \quad (22)$$

(Axelrod, 1979). The angle $\psi$ is the angle in the $X_2 - X_3$ plane between the positive $X_3$-axis and the transmission axis of the emission polarizer, measured clockwise as viewed from the positive $X_1$-axis. For $\psi = 0°$ and 90°, which correspond to $F_\parallel$ and $F_\perp$, respectively, Eq. 18 reduces to

$$F_\parallel(\rho, \gamma, \theta_{max}) = \frac{1}{2\pi(1 - \cos\theta_{max})}\int_{\theta=0}^{\theta_{max}}\int_{\phi=0}^{2\pi} f(\theta, \phi, \rho, \gamma, \theta_{max}) \cdot [K_a x_1^2 + K_b x_2^2 + K_c x_3^2]\sin\theta\, d\theta\, d\phi \quad (23)$$

$$F_\perp(\rho, \gamma, \theta_{max}) = \frac{1}{2\pi(1 - \cos\theta_{max})}\int_{\theta=0}^{\theta_{max}}\int_{\phi=0}^{2\pi} f(\theta, \phi, \rho, \gamma, \theta_{max}) \cdot [K_a x_1^2 + K_c x_2^2 + K_b x_3^2]\sin\theta\, d\theta\, d\phi. \quad (24)$$

Combining Eqs. 14–18 and integrating over $\theta$ and $\phi$ yields the polarized fluorescence intensity as a function of the degree of lipid order (in terms of the cone angle $\theta_{max}$) and position $(\rho, \gamma)$ on the membrane surface. The result is

$$F_\psi(\rho, \gamma, \theta_{max}) = K_a F_1 + (K_b\cos^2\psi + K_c\sin^2\psi)F_2 + (K_b\sin^2\psi + K_c\cos^2\psi)F_3 + 2(K_c - K_b)\sin\psi\cos\psi F_{2,3}, \quad (25a)$$

where

$$F_1 = \frac{1}{1 - \cos\theta_{max}}\sum_{\text{even } n=0}^{\infty}{}' \frac{1}{N_n[1 + n(n+1)D_w\tau]} \cdot \left\{\left(\frac{1}{4}U_n^2\cos^2\gamma + \frac{1}{2}T_nU_n\sin^2\gamma\right)\sin^2\rho + \left[\left(T_n^2 + \frac{1}{4}U_n^2\right)\sin^2\gamma\cos^2\gamma + \frac{1}{2}T_nU_n(\sin^4\gamma + \cos^4\gamma)\right]\cos^2\rho\right\} + \frac{1}{1 - \cos\theta_{max}} \cdot \sum_{\text{even } n=2}^{\infty}{}' \frac{(n-2)!}{(n+2)!}\frac{1}{8N_n^2[1 + n(n+1)D_w\tau]} \cdot V_n^2(-\cos^2\gamma\sin^2\rho + \sin^2\gamma\cos^2\gamma\cos^2\rho) \quad (25b)$$

$$F_2 = \frac{1}{1 - \cos\theta_{max}}\sum_{\text{even } n=0}^{\infty}{}' \frac{1}{N_n[1 + n(n+1)D_w\tau]} \cdot \left\{\left(\frac{1}{4}U_n^2\sin^2\gamma + \frac{1}{2}T_nU_n\cos^2\gamma\right)(\sin^4\rho + \cos^4\rho) + [T_n^2\cos^4\gamma + \frac{1}{4}U_n^2(\sin^4\gamma + 1) + T_nU_n\sin^2\gamma\cos^2\gamma]\sin^2\rho\cos^2\rho\right\} + \frac{1}{1 - \cos\theta_{max}}\sum_{\text{even } n=2}^{\infty}{}' \frac{(n-2)!}{(n+2)!} \cdot \frac{1}{8N_n^2[1 + n(n+1)D_w\tau]}V_n^2[-\sin^2\gamma(\sin^4\rho + \cos^4\rho) + (\sin^4\gamma - 4\sin^2\gamma + 1)\sin^2\rho\cos^2\rho] \quad (25c)$$

$$F_3 = \frac{1}{1 - \cos\theta_{max}}\sum_{\text{even } n=0}^{\infty}{}' \frac{1}{N_n[1 + n(n+1)D_w\tau]} \cdot \left\{\frac{1}{4}U_n^2\sin^4\rho + \left(T_n^2\cos^4\gamma + \frac{1}{4}U_n^2\sin^4\gamma + T_nU_n\sin^2\gamma\cos^2\gamma\right)\cos^4\rho + \left(\frac{1}{2}U_n^2\sin^2\gamma + T_nU_n\cos^2\gamma\right)\sin^2\rho\cos^2\rho\right\} + \frac{1}{1 - \cos\theta_{max}} \cdot \sum_{\text{even } n=2}^{\infty}{}' \frac{(n-2)!}{(n+2)!}\frac{1}{8N_n^2[1 + n(n+1)D_w\tau]} \cdot V_n^2(\sin^4\rho + \sin^4\gamma\cos^4\rho + 2\sin^2\gamma\sin^2\rho\cos^2\rho) \quad (25d)$$

$$F_{2,3} = \frac{1}{1 - \cos\theta_{max}}\sum_{\text{even } n=0}^{\infty}{}' \frac{1}{N_n[1 + n(n+1)D_w\tau]} \cdot \left\{\left(-\frac{1}{4}U_n^2 + \frac{1}{2}T_nU_n\right)\cos^2\gamma\sin^3\rho\cos\rho + \left[\left(T_n^2 - \frac{1}{2}T_nU_n\right)\cos^4\gamma + \left(-\frac{1}{4}U_n^2 + \frac{1}{2}T_nU_n\right) \cdot \sin^2\gamma\cos^2\gamma\right]\cos^3\rho\sin\rho\right\} + \frac{1}{1 - \cos\theta_{max}} \cdot \sum_{\text{even } n=2}^{\infty}{}' \frac{(n-2)!}{(n+2)!}\frac{1}{8N_n^2[1 + n(n+1)D_w\tau]} \cdot V_n^2(-\cos^2\gamma\sin^3\rho\cos\rho - \sin^2\gamma\cos^2\gamma\cos^3\rho\sin\rho). \quad (25e)$$

The above expression for polarized fluorescence intensity applies when the cone axis coincides with the normal to the membrane surface, i.e., the $X_3'$-axis (Fig. 1, *right*). If the bilayer exhibits a collective phospholipid tilt, as has been observed for gel-phase phosphatidylcholines, then a corresponding tilt of the cone axis should be used in the model of probe motion (Fig. 3). The generalized form of

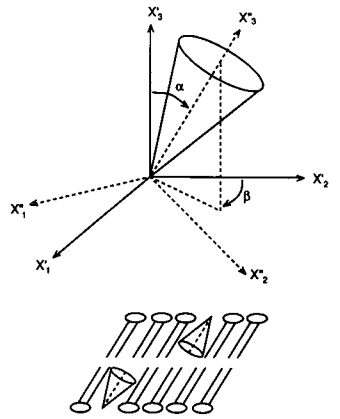


FIGURE 3. Model of phospholipid tilt. In the membrane (*primed*) frame, the $X'_3$-axis is normal to the membrane surface, defined by the $X'_1 - X'_2$ plane (see Fig. 1). In the cone (*doubly primed*) frame, the $X''_3$-axis is the symmetry axis of the cone in which the probe wobbles. A collective phospholipid tilt of angle $\alpha$ with respect to the bilayer normal is represented by an angle $\alpha$ between the $X''_3$- and $X'_3$-axes.

Eq. 25, in which a cone tilt of angle $\alpha$ is included, is presented in Appendix A. Because of the possibility that a fraction of probe molecules may be aligned parallel to the plane of the bilayer, an expression for polarized fluorescence intensity was obtained for this case as well, using a different model for probe rotational diffusion. The model employed, as well as the derivation of $F_\psi(\rho, \gamma)$, are outlined in Appendix B.

The fluorescence intensity recorded in each pixel in the two-dimensional fluorescence image is collected from a range of $\rho$ and $\gamma$ on the membrane surface that depends on pixel size and location. Therefore, the image intensity is given by

$$F_{\psi_{image}}(\theta_{max}) = \int_{\rho,\gamma} [(1 - c)F_{\psi_\perp}(\rho, \gamma, \theta_{max}) + cF_\psi(\rho, \gamma)] \sin \rho \, d\rho \, d\gamma, \quad (26)$$

where $c$ is the fraction of fluorophores aligned parallel to the bilayer plane, and the range of $\rho$ and $\gamma$ integration is determined by the area of interest in the image. For example, at the vesicle perimeter, which lies in the focal plane, $F_{\psi_\perp}(\rho, \gamma, \theta_{max})$ and $F_\psi(\rho, \gamma)$ are integrated over a range of $\gamma$ of $-\gamma_0 \le \gamma \le \gamma_0$ (Fig. 2), leaving the image intensity in each edge pixel a function of $\rho$ around the vesicle perimeter. At each pixel $\rho$ coordinate ($\equiv \rho_p$) we then integrate $F$ over the range $\rho_p - \tan^{-1}(x/2r) \le \rho \le \rho_p + \tan^{-1}(x/2r)$, where $x$ = pixel diameter and $r$ = vesicle radius, to obtain the fluorescence intensity for that pixel. For $x \ll r$, $\rho \approx \rho_p$ and integration over a range of $\rho$ is not necessary, in which case the image intensity around the vesicle perimeter as a function of $\rho$ is given by

$$F_{\psi_{image}}(\rho, \theta_{max}) = \int_{-\gamma_0}^{\gamma_0} [(1 - c)F_{\psi_\perp}(\rho, \gamma, \theta_{max}) + cF_\psi(\rho, \gamma)] \, d\gamma, \quad (27)$$

where $\gamma_0 = \cos^{-1}[(r - x)/r]$.

## EXPERIMENTAL METHODS

### Sample preparation

DPH, the cationic derivative TMA-DPH, and the phospholipid derivative DPH-PC were purchased from Molecular Probes, Inc. (Eugene, OR). POPC and DPPC, with respective phase transition temperatures of −5°C (Santaren et al., 1982) and 41°C (Mabrey and Sturtevant, 1976), were obtained from Avanti Polar Lipids, Inc. (Pelham, AL). Vesicles were prepared under dim light essentially as outlined by Mueller and co-workers (1983). A 0.5-ml solution of phospholipid (50 mg/ml) and probe (1:500 probe/lipid molar ratio) in chloroform/methanol (2:1, vol/vol) was spread on the bottom of a 100-ml Erlenmeyer flask and evaporated to dryness under a stream of argon gas. 100 ml of doubly distilled, deionized, and deoxygenated water was then slowly added to the flask, which was subsequently sealed under argon and incubated undisturbed in a 45°C water bath in the dark for 18–36 h. A few droplets from the resulting vesicle "cloud" near the bottom of the flask were pipetted onto a glass coverslip, which was then placed on the microscope stage and left undisturbed for 20–30 min at 25°C before viewing to allow for settling of the vesicles. Unilamellar vesicles were located and distinguished from multilamellar vesicles by phase contrast observation (Fig. 4). The range of vesicle diameters examined was 10–70 μm.

### Instrumentation

Fluorescence polarization measurements were made using an inverted microscope with epi-illumination optics (model IM-35; Carl Zeiss, Inc., Thornwood, NY) and an intensified silicon intensified target camera (model 66; Dage-MTI, Michigan City, IN) interfaced to a minicomputer, described previously (Lemasters et al., 1987; DiGuiseppi et al., 1985). The excitation light source was a xenon arc lamp, also from Carl Zeiss, Inc. A 365-nm bandpass filter, heat filter, and film polarizer were placed in the excitation light path. Fluorescence was observed through a 395-nm dichroic mirror in series with a 420-nm longpass filter and a rotatable polarizer in the emission path. All filters and polarizers were from Carl Zeiss, Inc. A 40×, 1.3 numerical aperture glycerol immersion objective (Nikon, Inc., Garden City, NJ) was used for all fluorescence polarization measurements. A rifle telescope (Carl Zeiss, Inc.) mounted between the microscope and camera allowed additional magnification of 1.5–6×.

### Image acquisition and processing

A set of fluorescence measurements on a single vesicle consisted of four images recorded with the emission polarizer transmission axis oriented at 0° (i.e., parallel), 45°, 90° (i.e., perpendicular), and 135° with respect to the positive $X_3$-axis (the excitation light polarization direction). The parallel orientation, which gave the brightest images, was used to

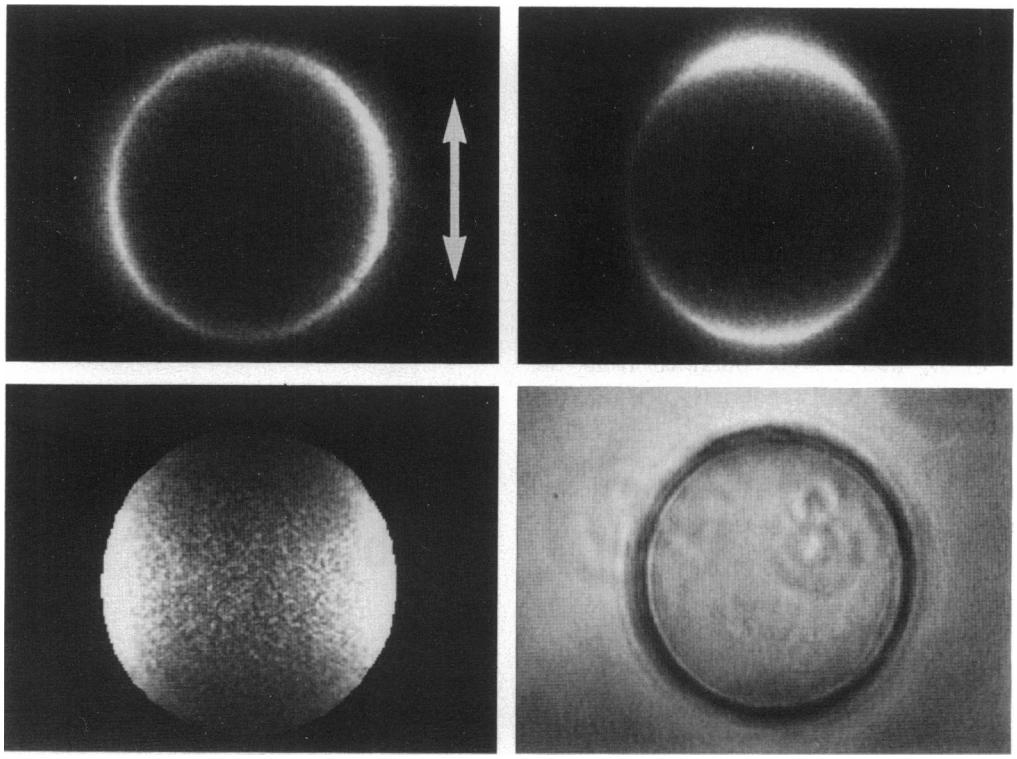

FIGURE 4 Image acquisition and processing. (*Upper left and right*) Fluorescence images, after background subtraction, of a DPH-labeled DPPC vesicle with the emission polarizer oriented perpendicular ($F_\perp$) and parallel ($F_\parallel$), respectively, to the excitation light polarization direction (indicated by the arrow). (*Lower left*) Ratio image, $F_\perp/F_\parallel \times 100$ (see Fig. 7, *upper right*, for the corresponding pseudocolor image). (*Lower right*) Phase contrast image. Vesicle diameter is 66 $\mu$m.

establish the camera amplifier gain and target voltage settings, which then remained fixed for each series of measurements. At settings of $\leq$70% of full scale, the range of recorded intensities fell within the linear response range of the camera (Tsay et al., 1990). Images obtained at each emission polarizer orientation were averages of 64 frames (2 s illumination time) and utilized the central 256 × 256 pixels of the 512 × 512 pixels comprising the field. Pixel diameter, determined with a stage micrometer, was typically 0.2 $\mu$m.

After background images were subtracted, fluorescence polarization ratios were computed from digitized image pairs on a pixel-by-pixel basis over the vesicle surface. Images were checked for alignment before ratioing to ensure that each pixel coordinate represented the same membrane location in each of the four fluorescence images. For display as $F_{90°}/F_{0°}$ ($= F_\perp/F_\parallel$) and $F_{135°}/F_{45°}$ ratio images, ratios were converted to gray levels (0–255) by using a multiplication factor of typically $M$ = 50 or 100 (Fig. 4). To better visualize changes in polarization ratio over the vesicle surface, ratio images were pseudocolored. The gray levels 1–255 were assigned color values of violet (low polarization ratio) to lavender to blue to green to yellow to red to white (high polarization ratio). Because of some residual signal in the extra-vesicular region of the fluorescence images even after background subtraction, the ratio images contained noise which sometimes made the vesicle edges difficult to identify. To overcome this problem a mapping program was applied to the fluorescence images before ratioing, in which the vesicle is outlined (mapped) and all pixel intensities outside of the map are set to zero. The ratio image then has zero intensity everywhere outside the vesicle.

## Corrections for effective birefringence of the microscope/imaging system

Intensity ratios were corrected for the polarization dependence of light transmission through the microscope emission optics, which was determined as follows. With the emission polarizer removed, and using transmitted light rather than epi-illumination, a 6.3× air objective, and an empty coverslip in place of a sample, initially unpolarized light of wavelength 425 nm was passed through a rotatable polarizer placed between the light source and the objective, in the $X_2 - X_3$ plane. Images were recorded at polarizer orientations of 0°, 45°, 90°, and 135° with respect to the positive $X_3$-axis. A 10% difference in response of the system to the 0° and 90° orientations was observed, and experimental $F_{90°}/F_{0°}$ ratio images were corrected accordingly.

Depolarization of the excitation beam by the 1.3 numerical aperture objective used for polarization measurements was also checked. A photomultiplier tube was mounted above the objective, near the sample plane, and the light transmission through the objective from 365-nm polarized epi-illumination was monitored as a polarizer placed between the objective and the photomultiplier was rotated. An empty coverslip and immersion fluid were used for this experiment. Depolarization was found to be negligible. This is not a surprising result because the excitation beam is defocused at the sample plane to provide uniform illumination over the entire field of view, thus minimizing high angle of convergence effects (Axelrod, 1989).

## RESULTS AND DISCUSSION

Theoretical fluorescence polarization ratios were calculated for the vesicle perimeter region, in the focal plane ($0° \leq \rho \leq 360°$ and $-\gamma_0 \leq \gamma \leq \gamma_0$, see Fig. 2), for several values of the cone angle $\theta_{max}$, in the absence or presence of a cone tilt of $\alpha = 30°$. Such a phospholipid tilt has been established by x-ray diffraction for hydrated DPPC below the gel-to-liquid-crystal phase transition temperature (Tardieu et al., 1973). The results are plotted in Figs. 5 and 6. Values of $D_w$ and $\tau$ were obtained from the literature (Stubbs et al., 1982; Prendergast et al., 1981). (The curves are much more sensitive to variations in $\theta_{max}$ than in $D_w$ or $\tau$.) The value of $\gamma_0 = 9.6°$ corresponds to a pixel diameter of 0.21 $\mu$m and vesicle radius of 15 $\mu$m (Fig. 2), typical of experimental values.

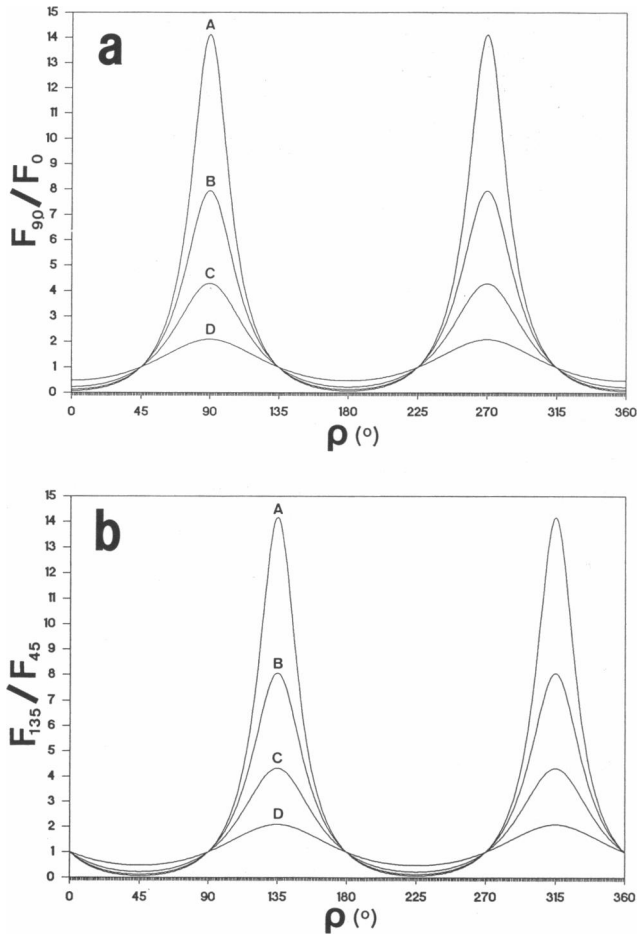


FIGURE 5 Theoretical polarization ratio $F_{90°}/F_{0°}$ ($=F_\perp/F_\parallel$) (*a*) or $F_{135°}/F_{45°}$ (*b*) vs. position on the vesicle perimeter in the absence of a cone tilt (i.e., $\alpha = 0°$). Cone angle $\theta_{max} = 16.7°$ (*A*), 27.5° (*B*), 40.9° (*C*), and 60.4° (*D*). Curves were generated from Eqs. 25 and 27 using $D_w\tau = 0.3$ (*A*, *B*) or 1.1 (*C*, *D*), $\gamma_0 = 9.6°$, and $c = 0$.

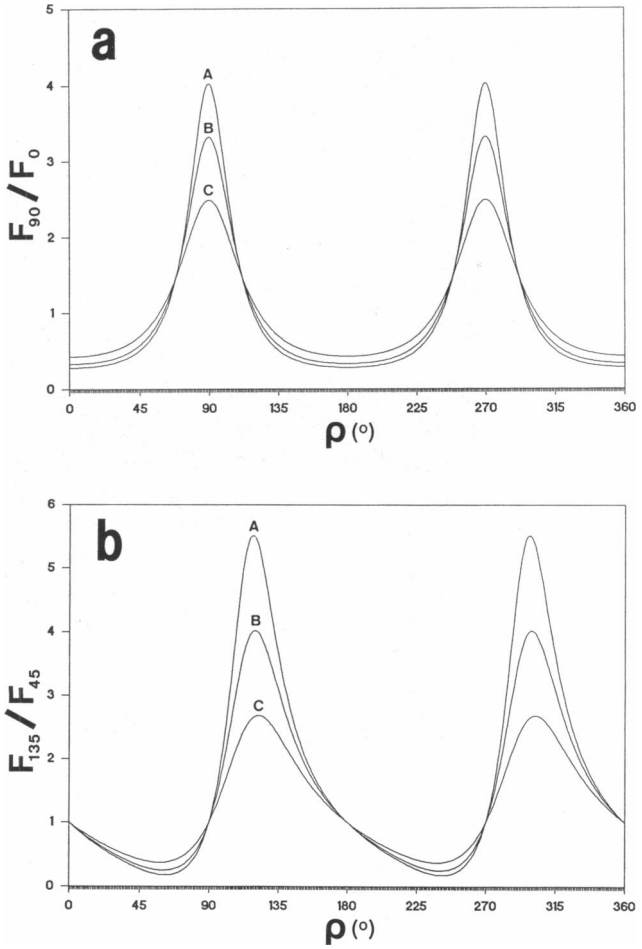


FIGURE 6 Theoretical polarization ratio $F_{90°}/F_{0°}$ ($=F_\perp/F_\parallel$) (*a*) or $F_{135°}/F_{45°}$ (*b*) vs. position on vesicle perimeter in the presence of a cone tilt of $\alpha = 30°$. Cone angle $\theta_{max} = 16.7°$ (*A*), 27.5° (*B*), and 40.9° (*C*). Curves were generated from Eqs. 27 and A6 using $D_w\tau = 0.3$ (*A*, *B*) or 1.1 (*C*), $\gamma_0 = 9.6°$, and $c = 0$.

As Fig. 5 *a* illustrates, the ratio $F_{90°}/F_{0°}$ goes through maxima and minima at 90° intervals around the vesicle perimeter. The values of the maxima range from 2.10 for $\theta_{max} = 60.4°$ (high degree of angular motional freedom) to 14.14 for $\theta_{max} = 16.7°$ (highly restricted motion). The values of the minima range from 0.48 for $\theta_{max} = 60.4°$ to 0.07 for $\theta_{max} = 16.7°$. A cone tilt of 30° (Fig. 6 *a*) has the effect of decreasing the maximum ratio values and increasing the minimum values. Regardless of a cone tilt, there are regions on the vesicle perimeter where $F_{90°}/F_{0°}$ is not sensitive to the value of $\theta_{max}$ (the regions where the curves intersect). Therefore, the degree of lipid order cannot be determined around the entire perimeter from measurements of $F_{90°}/F_{0°}$ alone. However, the ratio $F_{135°}/F_{45°}$ is most sensitive to $\theta_{max}$ in precisely those regions where $F_{90°}/F_{0°}$ is least sensitive, and vice versa (Figs. 5 *b*

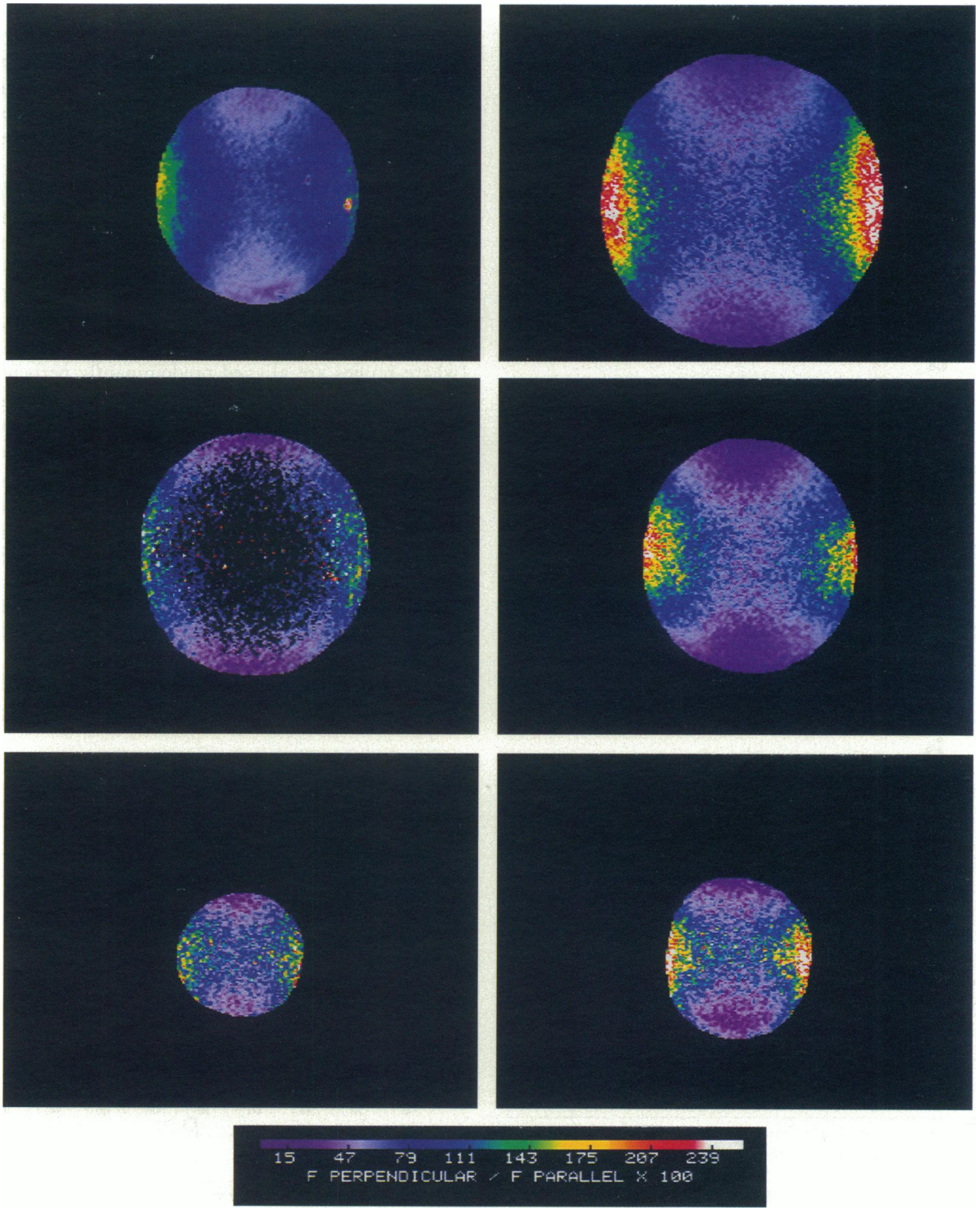


FIGURE 7 Pseudocolor ratio images, $F_\perp/F_\parallel \times 100$, of unilamellar vesicles composed of fluid-phase POPC (*left*) or gel-phase DPPC (*right*) and labeled with DPH (*top*), TMA-DPH (*center*), or DPH-PC (*bottom*). Vesicle diameters are (*clockwise from upper left*) 29, 66, 38, 21, 17, and 31 μm. The excitation light polarization direction is as shown in Fig. 4. Because the images are focused at the vesicle center (Fig. 1, *left*), intensity ratios in the central region contain contributions from both the upper and lower vesicle surfaces.

and 6 *b*), so that the two polarization ratios together can be used to map lipid order around the vesicle perimeter.

Pseudocolor $F_{90°}/F_{0°}$ ($F_\perp/F_\parallel$) ratio images of DPH, TMA-DPH, and DPH-PC in fluid-phase POPC and gel-phase DPPC vesicles are shown in Fig. 7. The changes in the polarization ratio around the vesicle perimeter are qualitatively similar to those predicted by the model (Figs. 5 *a* and 6 *a*). There are maxima at $\rho = 90°$ and 270° (*right and left sides of image,* respectively) and minima at $\rho = 0°$ and 180° (*top and bottom of image,* respectively). The maximum ratios are higher and the minimum ratios are lower in gel-phase compared with fluid-phase lipid. There are also regions between maxima and minima where the polarization ratio is much less sensitive to lipid phase state (e.g., $\rho$ = 40–60°). Vesicles did not always display completely symmetric fluorescence polarization patterns (e.g. Fig. 7, *upper left*) due to occasional surface irregularities, and those labeled with DPH-PC were generally smaller than those labeled with DPH or TMA-DPH.

For the vesicles shown in Fig. 7, the model curves that best fit the vesicle perimeter data are plotted along with representative data points in Figs. 8 (fluid-phase vesicles) and 9 (gel-phase vesicles), for $0° \leq \rho \leq 180°$. The average error in the measured $F_\perp/F_\parallel$, based on experiments performed on 5–10 vesicles of each sample composition, ranged from ~5% at $\rho = 0°$ and 180° to 10% at $\rho = 90°$ (where probes are aligned predominantly perpendicular to the excitation light polarization direction and are therefore only weakly excited). From the variation in image intensity between adjacent pixels, we estimate that we can measure the polarization ratio reasonably accurately in a 2 × 2 pixel area at the vesicle edges and a 5 × 5 pixel area at the out-of-focus center of the image. This corresponds to a surface spatial resolution of ~1 $\mu m^2$ for a vesicle of 30 $\mu$m diam.

The experimental results for both fluid- and gel-phase vesicles are well fit by physically reasonable models for probe orientation and dynamics. In the fluid phase, where the lipid acyl chains are highly disordered (particularly at the bilayer core), a high value of $\theta_{max}$ would be expected.

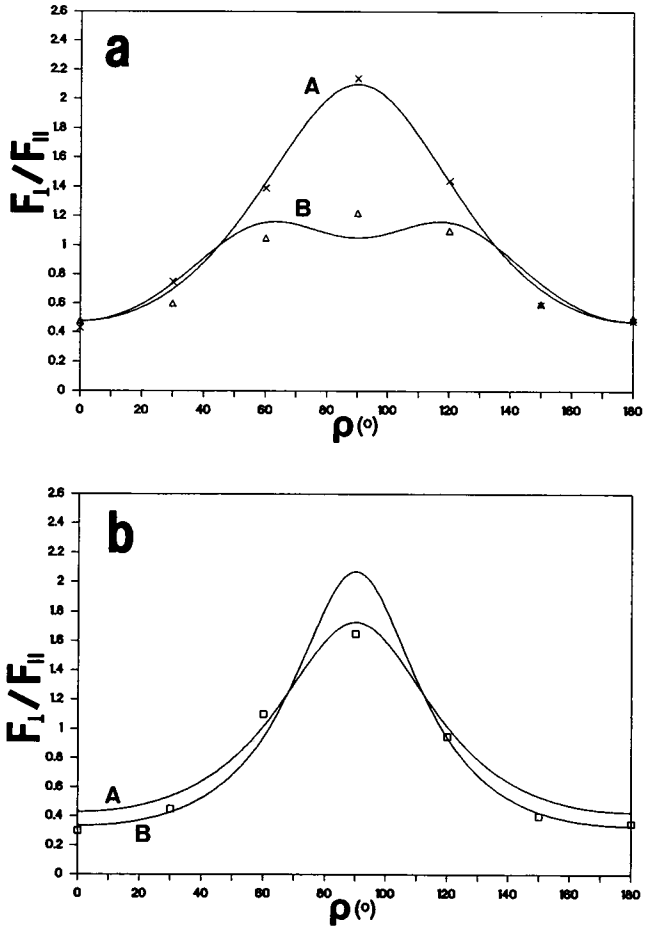


FIGURE 8 Comparison of experimental and theoretical $F_\perp/F_\parallel$ for fluid-phase vesicles. Representative data points from the vesicle edge region of the ratio images shown in Fig. 7 are plotted along with the model curves that best fit the data. (*a*) DPH (Δ) and DPH-PC (×) in POPC with model curves calculated from Eqs. 25, 27, and B11 using $\theta_{max}$ = 60.4°, $\alpha$ = 0°, $D_w\tau$ = 1.1, $\gamma_0$ = 12.5° (curve *A*) or 9.6° (curve *B*), $c$ = 0 (curve *A*) or 0.2 (curve *B*), and $D_R\tau$ = 1.0. (*b*) TMA-DPH (□) in POPC with model curves calculated from Eqs. 27, A6, and B11 using $\theta_{max}$ = 40.9° (curve *A*) or 27.5° (curve *B*), $\alpha$ = 30°, $D_w\tau$ = 0.6, $\gamma_0$ = 9.4°, $c$ = 0.1, and $D_R\tau$ = 1.0.

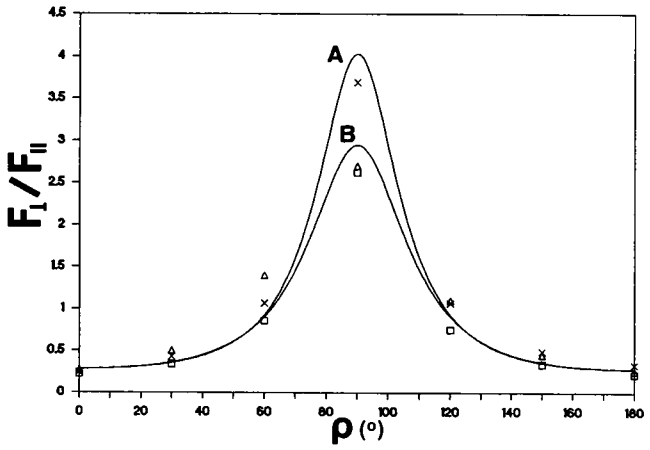


FIGURE 9 Comparison of experimental and theoretical $F_\perp/F_\parallel$ for gel-phase vesicles. Representative edge-region data points for the DPH (Δ)-, TMA-DPH (□)-, and DPH-PC (×)- labeled DPPC vesicles shown in Fig. 7 are plotted along with model curves calculated from Eqs. 27, A6, and B11 using $\theta_{max}$ = 16.7°, $\alpha$ = 30°, $D_w\tau$ = 0.3, $\gamma_0$ = 11.5° (curve *A*) or 9.6° (curve *B*), $c$ = 0 (curve *A*) or 0.05 (curve *B*), and $D_R\tau$ = 1.0.

We observe cone angles of 32 ± 4° for TMA-DPH, located near the more ordered headgroup region, and 60 ± 2° for DPH and DPH-PC. In the highly ordered gel phase, where a low value of $\theta_{max}$ would be expected, we find $\theta_{max} = 17 \pm 2°$ for all three probes. We also observe a component of DPH and TMA-DPH molecules aligned parallel to the plane of the bilayer of ~5% in gel-phase DPPC that increases to ~10% (TMA-DPH) or 20% (DPH) in fluid-phase POPC. The effect of an in-plane component is to decrease the ratio $F_\perp/F_\parallel$ in the vicinity of $\rho = 90°$ and 270° while leaving it virtually unchanged near $\rho = 0°$ and 180° (Figs. 8 *a* and 9). As Fig. 2 (*top*) illustrates, probes lying in the plane of the bilayer will be oriented perpendicular to the excitation light polarization direction (the $X_3$-axis) at $\rho = 0°$ and 180° and will contribute very little fluorescence, whereas at $\rho = 90°$ and 270° they will make a significant contribution to the fluorescence signal. The simplified model used for the in-plane component, in which $\theta$ is fixed at 90°, is the cause of the slight "dip" in the ratio $F_\perp/F_\parallel$ at $\rho = 90°$ shown in Fig. 8 *a* (curve *B*), which is not observed experimentally. However, the magnitude of the dip is small and corresponds roughly to the standard deviation in the measured polarization ratios at $\rho = 90°$, where the signal-to-noise ratio is lowest. No in-plane probe component would be expected for the phospholipid probe DPH-PC, and none is observed in either lipid phase.

The results are in good agreement with the literature. Cone angles of ≈35° for TMA-DPH and ≈60° for DPH in fluid-phase POPC, and 10–20° for DPH and TMA-DPH in gel-phase DPPC, have been reported (Engel and Prendergast, 1981; Stubbs et al., 1981) based on fluorometric studies. It has also be observed that a significant fraction of DPH, and to a much lesser extent TMA-DPH, molecules are aligned parallel to the bilayer plane, especially in fluid-phase lipid (Andrich and Vanderkooi, 1976; Ameloot et al., 1984; Mulders et al., 1986; Straume and Litman, 1987; Florine-Casteel and Feigenson, 1988).

The data for TMA-DPH in POPC and all three probes in DPPC are best fit by models which invoke a cone tilt of 30° that is fixed on the timescale of fluorescence (i.e., a few nanoseconds). This model also predicts $F_{135°}/F_{45°}$ polarization ratio maxima near $\rho = 120°$ and 300° which are greater than the $F_{90°}/F_{0°}$ ratio maxima at $\rho = 90°$ and 270° (Fig. 6). These predictions are borne out by the data, as Figs. 10 and 11 demonstrate. Allowing equally weighted tilt angles of $0 \leq \alpha \leq 30°$ during the time of collection of fluorescence results in poor fits of the data

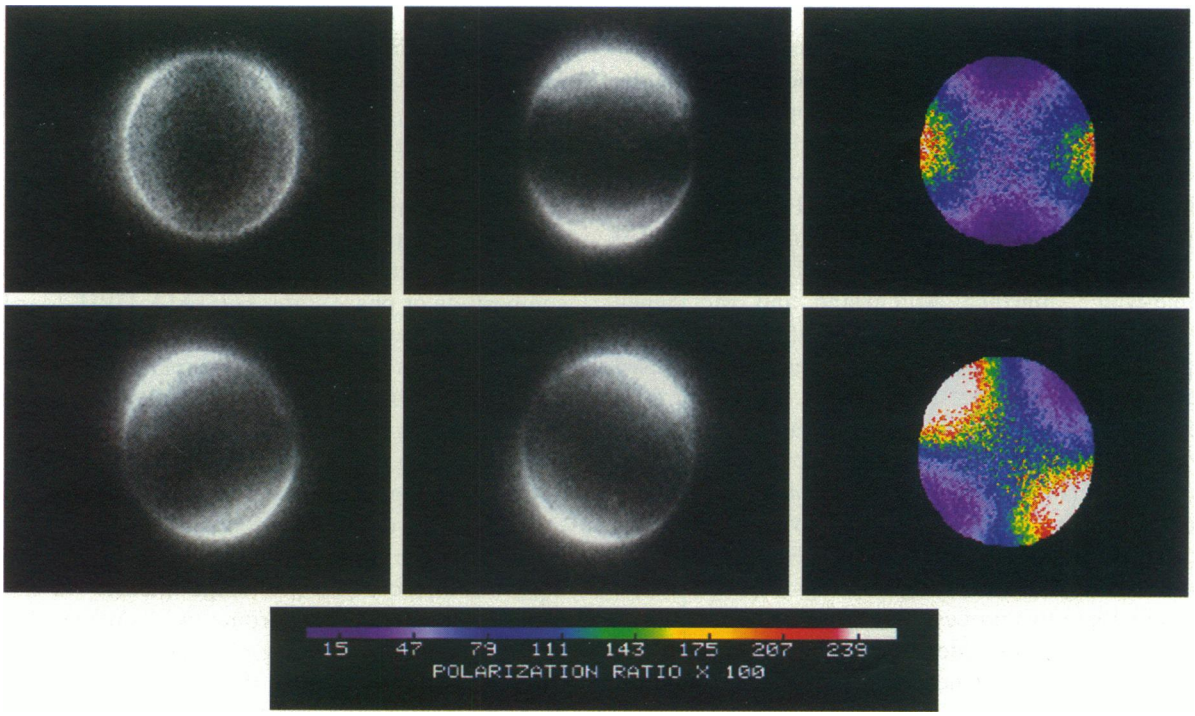


FIGURE 10 Fluorescence and ratio images of TMA-DPH in DPPC for emission polarizer orientations of $\psi = 0°$, 45°, 90°, and 135°. (*Top, left to right*) $F_{90°}$, $F_{0°}$, $F_{90°}/F_{0°} \times 100$ (also shown in Fig. 7). (*Bottom, left to right*) $F_{135°}$, $F_{45°}$, $F_{135°}/F_{45°} \times 100$. The excitation light polarization direction is as shown in Fig. 4.

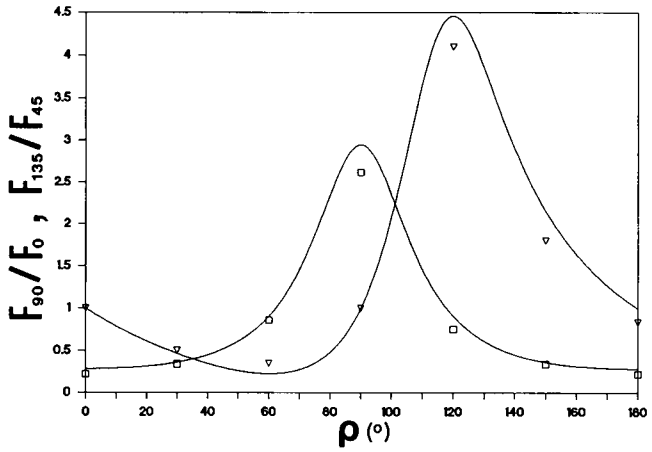


FIGURE 11 Comparison of experimental and theoretical polarization ratios $F_{90°}/F_{0°}$ and $F_{135°}/F_{45°}$. Representative values of $F_{90°}/F_{0°}$ (□) and $F_{135°}/F_{45°}$ (▽) from the data of Fig. 10 are plotted along with the corresponding theoretical curves calculated from Eqs. 27, A6, and B11 using $\theta_{max} = 16.7°$, $\alpha = 30°$, $D_w\tau = 0.3$, $\gamma_0 = 9.6°$, $c = 0.05$, and $D_R\tau = 1.0$.

(not shown). The gel-phase results are not surprising because bulk hydrated DPPC is known to adopt a collective tilt of ~30° below the phase transition temperature to accommodate the large headgroup. Our results indicate that this tilt is also present in cell-size unilamellar DPPC vesicles, and that reorientation of the phospholipid molecules takes place only in the $\beta$ direction (Fig. 3), on a timescale greater than the fluorescence lifetime of a few nanoseconds, with $\alpha$ remaining fixed at ~30°. The apparent tilt of TMA-DPH in fluid-phase POPC might be explained by a net tilt at or near the headgroup region of the bilayer because the charge group anchors this probe at the lipid-water interface. McFarland and McConnell (1971) reported a 30° tilt near the headgroup region of fluid-phase eggPC, with a lifetime of at least $10^{-8}$ s, based on electron spin resonance experiments, consistent with our results for POPC. An analysis of the anisotropy decay of TMA-DPH in POPC sonicated vesicles by van Langen and co-workers (1986) yielded two possible probe orientation distributions, one of which involved a collective molecular tilt. Because DPH and DPH-PC probe the bilayer core, a tilt of the headgroup region would not be reported by these two probes.

The degree of lipid order at a specific point on the vesicle perimeter cannot necessarily be uniquely determined from the four polarized fluorescence measurements $F_{0°}$, $F_{45°}$, $F_{90°}$, and $F_{135°}$ alone. For example, at $\rho = 90°$ the theory predicts $F_{90°}/F_{0°} \approx 4$ for the case in which $\theta_{max} = 40.9°$ in the absence of a cone tilt (Fig. 5) and also the case where $\theta_{max} = 16.7°$ in the presence of a cone tilt of 30° (Fig. 6). In a homogeneous vesicle, as is the case for this study, lipid order can be determined unambiguously by examining the polarization ratios at many locations (e.g., $0° \leq \rho \leq 180°$, as in Figs. 8, 9, and 11) and determining which model best fits the overall data. However, in a vesicle (or cell) of heterogeneous or unknown lipid composition, we need to be able to determine lipid order independently at each pixel location in the image. For the probe TMA-DPH, our results indicate that the symmetry axis about which the probe "wobbles" is tilted 30° from the bilayer normal regardless of lipid composition or phase state (Figs. 8 *b* and 9). Therefore, with this probe we can use the tilted cone model (Fig. 6) exclusively to determine phospholipid order (near the headgroup region) at any point on the vesicle perimeter from the ratios $F_{90°}/F_{0°}$ and $F_{135°}/F_{45°}$, without reference to other locations and without knowledge of the lipid composition. However, for DPH and DPH-PC, which probe the bilayer core, the presence of a net probe tilt will depend on lipid phase and composition because only certain lipids (e.g., DPPC) adopt a collective acyl chain tilt in the gel phase. Therefore, with these two probes, to determine lipid order unambiguously at a specific vesicle location, without reference to other locations, we need additional information. For a homogeneous vesicle, comparing the fluorescence polarization at different perimeter locations in the same image is equivalent to varying the excitation light polarization direction and examining only one location. For the theory we have described, a set of ratio images $F_{90°}/F_{0°}$ and $F_{135°}/F_{45°}$ obtained with the excitation light polarization direction along the $X_2$-axis in addition to the $X_3$-axis, for a total of eight fluorescence images rather than four, should be sufficient to uniquely determine lipid order as a function of position on the vesicle perimeter, for any of the probes, with no prior knowledge of lipid composition or phase state. For TMA-DPH, four fluorescence images will suffice, assuming that the symmetry axis maintains a constant tilt relative to the bilayer normal. (We observe typically a 3–5% loss of fluorescence after acquiring four fluorescence images, due to probe photobleaching, therefore it is important to minimize the number of images required.)

In moving from the edges of the vesicle image toward the center, the observed fluorescence becomes increasingly out of focus and the image intensity in each pixel contains contributions from two surface locations, $(\rho, +\gamma)$ and $(\rho, -\gamma)$ (Fig. 1, *left*). In that sense, the surface spatial resolution is limited. Also, at $\gamma = 90°$, probe molecules are aligned, on average, along the optical axis where the probability of excitation is low and fluorescence polarization ratios are not very sensitive to the degree of lipid order, as Fig. 7 illustrates. However, despite these limitations, the method presented here has

several advantages. For example, it requires only a limited number of images, which is important in minimizing photodamage to probes or cells and in maximizing temporal resolution. It is also experimentally less complicated than time-resolved techniques. The data analysis does make use of a model for probe rotational diffusion. However, the number of physically reasonable models for rod-shaped probes in a membrane environment is quite limited. Burghardt (1984) has presented a generalized model-independent method for obtaining the angular potential restricting probe motion, from steady-state fluorescence polarization measurements. However, for cases where the characteristic rotational correlation time is on the order of the fluorescence lifetime, as is the case for DPH probes in lipid bilayers, the model-independent method gives only an approximation to the true potential. It also requires analysis of data collected at many polarizer orientations.

## SUMMARY AND CONCLUSIONS

Using the method outlined above, we were able to measure with reasonable accuracy the degree of phospholipid acyl chain order in cell-size liposomes with a spatial resolution of $\sim 1\ \mu m^2$, as well as to determine the fraction of probe molecules aligned parallel to the bilayer plane, an important factor in probe selection. We were also able to verify a 30° collective phospholipid tilt in cell-size gel-phase DPPC vesicles which corresponds to that observed in bulk lipid, and to corroborate the existence of a tilt at or near the phospholipid headgroup region in fluid-phase POPC vesicles.

This study utilized single vesicles of homogeneous composition and hence the results could have been obtained using a focused spot, as was done by Axelrod (1979), rather than an imaging system. However, there are many instances in which the ability to rapidly analyze the entire field of view from one or two image pairs would be invaluable. The polarization ratio images shown in Figs. 7 and 10, along with the theoretical curves presented in Figs. 5 and 6, serve to illustrate, for various combinations of excitation and emission polarizer orientations, the regions of the ratio image that are most (and least) sensitive to the degree of lipid order, as well as the spatial resolution that can be expected for a spherical, cell-size object. Possible applications of the technique include the monitoring of lipid phase separation and domain formation in a vesicle of heterogeneous lipid composition or in the contact region of fusing vesicles or cells. An application we are currently pursuing is the measurement of lipid order in single cell plasma membrane blebs, which are structurally similar to liposomes, during hypoxic and toxic injury.

## APPENDIX A

### Polarized fluorescence intensity as a function of lipid order, membrane surface location, and phospholipid tilt angle

In the cone frame (doubly primed, see Fig. 3), a unit magnitude absorption dipole moment will have components $(x_1'', x_2'', x_3'') = (\sin\theta' \sin\phi', \sin\theta' \cos\phi', \cos\theta')$. Transformation to the laboratory frame by a series of coordinate axis rotations yields absorption dipole components

$$x_1 = \cos\gamma \cos\beta \sin\theta' \sin\phi' + \cos\gamma \sin\beta(\cos\alpha \sin\theta' \cos\phi' + \sin\alpha \cos\theta') - \sin\gamma \sin\alpha \sin\theta' \cos\phi' + \sin\gamma \cos\alpha \cos\theta' \quad \text{(A1)}$$

$$x_2 = -\cos\rho \sin\beta \sin\theta' \sin\phi' + \cos\rho \cos\beta (\cos\alpha \sin\theta' \cos\phi' + \sin\alpha \cos\theta') - \sin\rho \sin\gamma \cos\beta \sin\theta' \sin\phi' - \sin\rho \sin\gamma \sin\beta \cdot (\cos\alpha \sin\theta' \cos\phi' + \sin\alpha \cos\theta') - \sin\rho \cos\gamma \sin\alpha \sin\theta' \cos\phi' + \sin\rho \cos\gamma \cos\alpha \cos\theta' \quad \text{(A2)}$$

$$x_3 = \sin\rho \sin\beta \sin\theta' \sin\phi' - \sin\rho \cos\beta (\cos\alpha \sin\theta' \cos\phi' + \sin\alpha \cos\theta') - \cos\rho \sin\gamma \cos\beta \sin\theta' \sin\phi' - \cos\rho \sin\gamma \sin\beta \cdot (\cos\alpha \sin\theta' \cos\phi' + \sin\alpha \cos\theta') - \cos\rho \cos\gamma \cdot \sin\alpha \sin\theta' \cos\phi' + \cos\rho \cos\gamma \cos\alpha \cos\theta'. \quad \text{(A3)}$$

The emission dipole components $x_i(\theta, \phi, \alpha, \beta, \rho, \gamma)$ are obtained by replacing $\theta'$ and $\phi'$ with $\theta$ and $\phi$. For $\alpha = \beta = 0°$, i.e., in the absence of a cone tilt, Eqs. A1–A3 reduce to text Eqs. 11–13. Substituting Eq. A3 into text Eq. 10 yields the probe excited-state orientation distribution for the case of a cone axis orientation $(\alpha, \beta)$ that remains fixed during the excited-state lifetime,

$$f(\theta, \phi, \alpha, \beta, \rho, \gamma, \theta_{max}) = \sum_{\text{even } n=0}^{\infty}{}' \frac{P_n(\cos\theta)}{N_n[1 + n(n+1)D_w\tau]} \cdot \left\{ T_n \left[ \sin^2\rho \sin^2\alpha \cos^2\beta + \cos^2\rho \cdot \left( \sin^2\gamma \sin^2\alpha \sin^2\beta + \cos^2\gamma \cos^2\alpha - \frac{1}{2} \sin 2\gamma \sin 2\alpha \sin\beta \right) + \frac{1}{2} \sin 2\rho \, (\sin\gamma \sin^2\alpha \sin 2\beta - \cos\gamma \sin 2\alpha \cos\beta) \right] + \frac{1}{2} U_n \left[ \sin^2\rho \, (\sin^2\beta + \cos^2\alpha \cos^2\beta) + \cos^2\rho \right.$$

$$\cdot (\sin^2\gamma\cos^2\beta + \sin^2\gamma\cos^2\alpha\sin^2\beta + \cos^2\gamma\sin 2\alpha + \sin 2\gamma\sin 2\alpha\sin\beta) - \frac{1}{2}\sin 2\rho\,(\sin\gamma\sin^2\alpha\sin 2\beta - \cos\gamma\sin 2\alpha\cos\beta)\Big]\Big\} + \sum_{\text{even } n=2}^{\infty}{}' \frac{(n-2)!}{(n+2)!}\frac{P_n^2(\cos\theta)}{2N_n^2[1+n(n+1)D_w\tau]} \cdot V_n\Big\{\cos 2\phi\Big[\sin^2\rho\,(\cos^2\alpha\cos^2\beta - \sin^2\beta) + \cos^2\rho\Big(\sin^2\gamma\cos^2\alpha\sin^2\beta - \sin^2\gamma\cos^2\beta + \cos^2\gamma\sin^2\alpha + \frac{1}{2}\sin 2\gamma\sin 2\alpha\sin\beta\Big) + \frac{1}{2}\sin 2\rho\,(\sin\gamma\sin 2\beta + \sin\gamma\cos^2\alpha\sin 2\beta + \cos\gamma\sin 2\alpha\cos\beta)\Big] + \sin 2\phi\,[-\sin^2\rho\cos\alpha\sin 2\beta + \cos^2\rho \cdot (\sin^2\gamma\cos\alpha\sin 2\beta + \sin 2\gamma\sin\alpha\cos\beta) + \sin 2\rho\,(\sin\gamma\cos\alpha\cos 2\beta - \cos\gamma\sin\alpha\sin\beta)]\Big\}. \quad \text{(A4)}$$

Eq. A4, which reverts to text Eq. 14 for $\alpha = \beta = 0°$, represents the generalized form of the excited-state orientation distribution function. The corresponding polarized fluorescence intensity, normalized over the region $0 \le \theta \le \theta_{max}$ and $0 \le \phi \le 2\pi$, is given by

$$F_\psi(\rho,\gamma,\theta_{max}) = \frac{1}{2\pi(1-\cos\theta_{max})} \cdot \int_\alpha\int_\beta\int_{\theta=0}^{\theta_{max}}\int_{\phi=0}^{2\pi} f(\theta,\phi,\alpha,\beta,\rho,\gamma,\theta_{max})[K_a x_1^2 + (K_b\cos^2\psi + K_c\sin^2\psi)x_2^2 + (K_b\sin^2\psi + K_c\cos^2\psi)x_3^2 + 2(K_c - K_b)\sin\psi\cos\psi\,x_2x_3]\sin\theta\,d\theta\,d\phi\sin\alpha\,d\alpha\,d\beta, \quad \text{(A5)}$$

where $x_1$, $x_2$, and $x_3$ are given by Eqs. A1–A3 except with $\theta$ and $\phi$ substituted for $\theta'$ and $\phi'$. The range of $\alpha$ and $\beta$ integration depends on the particular model to be tested. We consider specifically the situation in which the phospholipid tilt angle $\alpha$ remains fixed during the time of collection of fluorescence, whereas all $\beta$ orientations are equally likely. Combining Eqs. A4 and A5 and integrating over $\theta$, $\phi$, and $\beta$, where $0 \le \beta \le 2\pi$, yields

$$F_{\psi_n}(\rho,\gamma,\theta_{max}) = K_a F_{1_n} + (K_b\cos^2\psi + K_c\sin^2\psi)F_{2_n} + (K_b\sin^2\psi + K_c\cos^2\psi)F_{3_n} + 2(K_c - K_b)\sin\psi\cos\psi\,F_{2,3_n}, \quad \text{(A6a)}$$

where

$$F_{1_n} = \frac{1}{1-\cos\theta_{max}}\sum_{\text{even } n=0}^{\infty}{}'\frac{1}{N_n[1+n(n+1)D_w\tau]} \cdot \Big(\Big\{T_n^2\Big(\frac{1}{2}\sin^2\alpha\cos^2\alpha\sin^2\gamma + \frac{1}{8}\sin^4\alpha\cos^2\gamma\Big) + U_n^2\Big[\frac{1}{8}\sin^2\alpha\,(\cos^2\alpha+1)\sin^2\gamma + \frac{1}{32}(\cos^4\alpha + 6\cos^2\alpha + 1)\cos^2\gamma\Big] + T_nU_n\Big[\frac{1}{4}(\sin^4\alpha + \cos^4\alpha + \cos^2\alpha)\sin^2\gamma + \frac{1}{8}\sin^2\alpha\,(\cos^2\alpha+3)\cos^2\gamma\Big]\Big\}\sin^2\rho + \Big\{T_n^2\Big[\frac{1}{2}\sin^2\alpha\cos^2\alpha\,(\sin^4\gamma + \cos^4\gamma) + \Big(\frac{3}{8}\sin^4\alpha + 3\cos^4\alpha - 2\cos^2\alpha\Big)\sin^2\gamma\cos^2\gamma\Big] + U_n^2\Big[\frac{1}{8}\sin^2\alpha\,(\cos^2\alpha+1)(\sin^4\gamma + \cos^4\gamma) + \frac{1}{32}(27\cos^4\alpha - 30\cos^2\alpha + 11)\sin^2\gamma\cos^2\gamma\Big] + T_nU_n\Big[\frac{1}{4}(\sin^4\alpha + \cos^4\alpha + \cos^2\alpha)(\sin^4\gamma + \cos^4\gamma) + \frac{1}{8}\sin^2\alpha\,(27\cos^2\alpha + 1)\sin^2\gamma\cos^2\gamma\Big]\Big\}\cos^2\rho\Big) + \frac{1}{1-\cos\theta_{max}}\sum_{\text{even } n=2}^{\infty}{}'\frac{(n-2)!}{(n+2)!}\frac{1}{8N_n^2[1+n(n+1)D_w\tau]}V_n^2 \cdot \Big\{\Big[-\frac{1}{2}\sin^4\alpha\sin^2\gamma + \frac{1}{8}(\cos^4\alpha - 10\cos^2\alpha + 1)\cos^2\gamma\Big]\sin^2\rho + \Big[-\frac{1}{2}\sin^4\alpha\,(\sin^4\gamma + \cos^4\gamma) + \frac{1}{8}(23\cos^4\alpha - 6\cos^2\alpha - 9)\sin^2\gamma\cos^2\gamma\Big]\cos^2\rho\Big\} \quad \text{(A6b)}$$

$$F_{2_n} = \frac{1}{1-\cos\theta_{max}}\sum_{\text{even } n=0}^{\infty}{}'\frac{1}{N_n[1+n(n+1)D_w\tau]} \cdot \Big(\Big\{T_n^2\Big(\frac{1}{2}\sin^4\alpha\sin^2\gamma + \sin^2\alpha\cos^2\gamma\Big) + U_n^2\Big[\frac{1}{32}(\cos^4\alpha + 6\cos^2\alpha + 1)\sin^2\gamma + \frac{1}{8}\sin^2\alpha \cdot (\cos^2\alpha+1)\cos^2\gamma\Big] + T_nU_n\Big[\frac{1}{16}\sin^2\alpha\,(5\cos^2\alpha+7)\sin^2\gamma + \frac{1}{4}(2\sin^4\alpha + \cos^4\alpha + \cos^2\alpha)\cos^2\gamma\Big]\Big\}\sin^4\rho + \Big\{T_n^2\Big(\frac{1}{8}\sin^4\alpha\sin^2\gamma + \frac{1}{2}\sin^2\alpha\cos^2\alpha\cos^2\gamma\Big) + U_n^2\Big[\frac{1}{32}(\cos^4\alpha + 6\cos^2\alpha + 1)\sin^2\gamma + \frac{1}{8}\sin^2\alpha\,(\cos^2\alpha+1)\cos^2\gamma\Big] + T_nU_n\Big[\frac{1}{8}\sin^2\alpha\,(\cos^2\alpha+3)\sin^2\gamma$$

$$+\frac{1}{4}(\sin^4\alpha+\cos^4\alpha+\cos^2\alpha)\cos^2\gamma\Big]\Big\}\cos^4\rho$$

$$+\Big\{T_n^2\Big[\frac{3}{8}\sin^4\alpha\sin^4\gamma+\cos^4\alpha\cos^4\gamma$$

$$+\sin^2\alpha\cos^2\alpha\cos^2\gamma(3\sin^2\gamma-2)+\frac{1}{2}\sin^4\alpha\cos^2\gamma\Big]$$

$$+U_n^2\Big[\frac{1}{32}(3\cos^4\alpha+2\cos^2\alpha+3)(\sin^4\gamma+1)$$

$$+\frac{1}{4}\sin^4\alpha\cos^4\alpha+\frac{1}{4}\sin^2\alpha(3\cos^2\alpha+1)\sin^2\gamma\cos^2\gamma$$

$$-\frac{1}{8}\sin^4\alpha\sin^2\gamma-\frac{1}{2}\sin^2\alpha\cos^2\alpha\cos^2\gamma\Big]$$

$$+T_nU_n\Big[\frac{1}{8}\sin^2\alpha(3\cos^2\alpha+1)\sin^4\gamma+\sin^2\alpha\cos^2\alpha\cos^4\gamma$$

$$+\frac{1}{2}(\sin^4\alpha+5\cos^4\alpha-3\cos^2\alpha)\sin^2\gamma\cos^2\gamma$$

$$+\frac{1}{2}\sin^4\alpha\sin^2\gamma+2\sin^2\alpha\cos^2\alpha\cos^2\gamma\Big]\Big\}\sin^2\rho\cos^2\rho\Big)$$

$$+\frac{1}{1-\cos\theta_{\max}}\sum_{\text{even}\,n-2}^{\infty\prime}\frac{(n-2)!}{(n+2)!}\frac{1}{8N_n^2[1+n(n+1)D_w\tau]}$$

$$\cdot V_n^2\Big\{\Big[\frac{1}{8}(\cos^4\alpha-10\cos^2\alpha+1)\sin^2\gamma-\frac{1}{2}\sin^4\alpha\cos^2\gamma\Big]$$

$$\cdot(\sin^4\rho+\cos^4\rho)+\Big[\frac{1}{8}(3\cos^4\alpha+2\cos^2\alpha+3)(\sin^4\gamma+1)$$

$$+\sin^4\alpha\cos^4\gamma+\sin^2\alpha(3\cos^2\alpha+1)\sin^2\gamma\cos^2\gamma$$

$$-\frac{1}{2}(\cos^4\alpha+6\cos^2\alpha+1)\sin^2\gamma$$

$$-2\sin^2\alpha(\cos^2\alpha+1)\cos^2\gamma\Big]\sin^2\rho\cos^2\rho\Big\} \quad \text{(A6c)}$$

$$F_{3,n}=\frac{1}{1\cos\theta_{\max}}\sum_{\text{even}\,n-0}^{\infty\prime}\frac{1}{N_n[1+n(n+1)D_w\tau]}$$

$$\cdot\Big(\Big[\frac{1}{2}T_n^2\sin^4\alpha+\frac{1}{32}U_n^2(3\cos^4\alpha+2\cos^2\alpha+3)$$

$$+\frac{1}{16}T_nU_n\sin^2\alpha(7\cos^2\alpha+5)\Big]\sin^4\rho+\Big\{T_n^2\Big(\frac{3}{8}\sin^4\alpha\sin^4\gamma$$

$$+\cos^4\alpha\cos^4\gamma+3\sin^2\alpha\cos^2\alpha\sin^2\gamma\cos^2\gamma\Big)$$

$$+U_n^2\Big[\frac{1}{32}(3\cos^4\alpha+2\cos^2\alpha+3)$$

$$\cdot\sin^4\gamma+\frac{1}{4}\sin^4\alpha\cos^4\gamma+\frac{1}{4}\sin^2\alpha(3\cos^2\alpha+1)\sin^2\gamma\cos^2\gamma\Big]$$

$$+T_nU_n\Big[\frac{1}{8}\sin^2\alpha(3\cos^2\alpha+1)\sin^4\gamma+\sin^2\alpha\cos^2\alpha\cos^4\gamma$$

$$+\frac{1}{2}(\sin^4\alpha+5\cos^4\alpha-3\cos^2\alpha)\sin^2\gamma\cos^2\gamma\Big]\Big\}\cos^4\rho$$

$$+\Big\{T_n^2\Big(\frac{9}{8}\sin^4\alpha\sin^2\gamma+\frac{7}{2}\sin^2\alpha\cos^2\alpha\cos^2\gamma\Big)$$

$$+U_n^2\Big[\frac{1}{16}(3\cos^4\alpha+2\cos^2\alpha+3)\sin^2\gamma+\frac{1}{4}\sin^2\alpha$$

$$\cdot(3\cos^2\alpha+1)\cos^2\gamma\Big]+T_nU_n\Big[\frac{5}{16}\sin^2\alpha(3\cos^2\alpha+1)\sin^2\gamma$$

$$+\frac{1}{4}(13\cos^4\alpha-12\cos^2\alpha+3)\cos^2\gamma\Big]\Big\}\sin^2\rho\cos^2\rho\Big)$$

$$+\frac{1}{1-\cos\theta_{\max}}\sum_{\text{even}\,n-2}^{\infty\prime}\frac{(n-2)!}{(n+2)!}\frac{1}{8N_n^2[1+n(n+1)D_w\tau]}$$

$$\cdot V_n^2\Big\{\Big[\frac{1}{8}(3\cos^4\alpha+2\cos^2\alpha+3)\sin^4\rho$$

$$+\Big[\frac{1}{8}(3\cos^4\alpha+2\cos^2\alpha+3)\sin^4\gamma+\sin^4\alpha\cos^4\gamma$$

$$+\sin^2\alpha(3\cos^2\alpha+1)\sin^2\gamma\cos^2\gamma\Big]$$

$$\cdot\cos^4\rho+\Big[\frac{1}{4}(3\cos^4\alpha+2\cos^2\alpha+3)\sin^2\gamma$$

$$+\sin^2\alpha(3\cos^2\alpha+1)\cos^2\gamma\Big]\sin^2\rho\cos^2\rho\Big\} \quad \text{(A6d)}$$

$$F_{2,3,n}=\frac{1}{1-\cos\theta_{\max}}\sum_{\text{even}\,n-0}^{\infty\prime}\frac{1}{N_n[1+n(n+1)D_w\tau]}$$

$$\cdot\Big(\Big\{T_n^2\Big[\frac{1}{4}\sin^4\alpha(3\sin^2\gamma-2)+2\sin^2\alpha\cos^2\alpha\cos^2\gamma\Big]+\frac{1}{32}U_n^2$$

$$\cdot(-15\cos^4\alpha+6\cos^2\alpha+1)\cos^2\gamma+T_nU_n\Big[-\frac{1}{8}\sin^4\alpha\sin^2\gamma$$

$$+\frac{1}{16}(35\cos^4\alpha-30\cos^2\alpha+3)\cos^2\gamma\Big]\Big\}\sin^3\rho\cos\rho$$

$$+\Big\{\frac{1}{8}T_n^2[(35\cos^4\alpha-30\cos^2\alpha+3)\cos^4\gamma$$

$$+(-15\cos^4\alpha+18\cos^2\alpha-3)\cos^2\gamma]$$

$$+\frac{1}{32}U_n^2[(35\cos^4\alpha-30\cos^2\alpha+3)\cos^4\gamma$$

$$-(3\cos^4\alpha+2\cos^2\alpha+3)\cos^2\gamma]$$

$$+\frac{1}{8}T_nU_n[(-35\cos^4\alpha+30\cos^2\alpha-3)\cos^4\gamma$$

$$+(15\cos^4\alpha-12\cos^2\alpha+1)\cos^2\gamma]\Big\}\cos^3\rho\sin\rho\Big)$$

$$+\frac{1}{1-\cos\theta_{\max}}\sum_{\text{even}\,n-2}^{\infty\prime}\frac{(n-2)!}{(n+2)!}\frac{1}{8N_n^2[1+n(n+1)D_w\tau]}$$

$$\cdot V_n^2\Big\{\frac{1}{8}(-15\cos^4\alpha+6\cos^2\alpha+1)\cos^2\gamma\sin^3\rho\cos\rho$$

$$+ \frac{1}{8}\left[(35\cos^4\alpha - 30\cos^2\alpha + 3)\cos^4\gamma + (-15\cos^4\alpha + 6\cos^2\alpha + 1)\cos^2\gamma\right]\cos^3\rho\sin\rho\Big\}. \quad \text{(A6e)}$$

Eq. A6 reverts to text Eq. 25 for $\alpha = \beta = 0°$.

## APPENDIX B

## Derivation of theoretical orientation-dependent fluorescence polarization for probes aligned parallel to the bilayer plane

Probe molecules residing between the inner and outlet leaflets of the bilayer, with absorption/emission dipoles oriented parallel to the bilayer plane, are treated as follows. Angles $\theta'$ and $\theta$ (Fig. 1, *right*) are fixed at 90° so that probe rotation in the $X_1' - X_2'$ plane is defined by the diffusion equation

$$\frac{\partial p(\phi', t'|\phi, t)}{\partial t} = D_R \frac{\partial^2 p(\phi', t'|\phi, t)}{\partial \phi^2} \quad \text{(B1)}$$

with the delta-function initial condition

$$p(\phi', t'|\phi, t') = \delta(\phi - \phi'). \quad \text{(B2)}$$

$D_R$ is the rotational diffusion coefficient. The solution can be written as

$$p(\phi', t'|\phi, t) = \frac{1}{2\pi} + \frac{1}{\pi}\sum_{n=1}^{\infty} e^{-n^2 D_R(t-t')}\cos n(\phi - \phi'). \quad \text{(B3)}$$

For excitation light polarized in the $X_3$ direction, the probe excited-state orientation distribution is given by

$$f(\phi, \rho, \gamma) = \frac{1}{\tau}\int_{\phi'=0}^{2\pi}\int_{(t-t')=0}^{\infty} x_3^2(\phi', \rho, \gamma) \cdot p(\phi', t'|\phi, t)e^{-(t-t')/\tau}\, d\phi'\, d(t - t'), \quad \text{(B4)}$$

where

$$x_3(\phi', \rho, \gamma) = -\sin\rho\cos\phi' - \cos\rho\sin\gamma\sin\phi', \quad \text{(B5)}$$

found by setting $\theta' = 90°$ in text Eq. 13. Combining Eqs. B3–B5 yields

$$f(\phi, \rho, \gamma) = \frac{1}{2}(\sin^2\rho + \cos^2\rho\sin^2\gamma) + \frac{1}{2(1 + 4D_R\tau)} \cdot [\cos 2\phi(\sin^2\rho - \cos^2\rho\sin^2\gamma) + \sin 2\phi\sin 2\rho\sin\gamma]. \quad \text{(B6)}$$

For orientation $\psi$ of the emission polarizer (defined in the text), the fluorescence collected from the membrane surface location $(\rho,\gamma)$, normalized over the region $0 \le \phi \le 2\pi$, is given by

$$F_\psi(\rho, \gamma) = \frac{1}{2\pi}\int_{\phi=0}^{2\pi} f(\phi, \rho, \gamma)[K_a x_1^2 + (K_b\cos^2\psi + K_c\sin^2\psi)x_2^2 + (K_b\sin^2\psi + K_c\cos^2\psi)x_3^2 + 2(K_c - K_b)\sin\psi\cos\psi x_2 x_3]\, d\phi, \quad \text{(B7)}$$

where the components $x_i(\phi,\rho,\gamma)$ of a unit magnitude emission dipole moment in the laboratory frame are

$$x_1 = \cos\gamma\sin\phi \quad \text{(B8)}$$

$$x_2 = \cos\rho\cos\phi - \sin\rho\sin\gamma\sin\phi \quad \text{(B9)}$$

$$x_3 = -\sin\rho\cos\phi - \cos\rho\sin\gamma\sin\phi, \quad \text{(B10)}$$

found by substituting $\theta$ and $\phi$ for $\theta'$ and $\phi'$ in text Eqs. 11–13 and setting $\theta$ equal to 90°. $K_a$, $K_b$, and $K_c$ are defined in text Eqs. 19–21. Combining Eqs. B6–B10 and integrating over $\phi$ yields the following expression for polarized fluorescence intensity as a function of position on the membrane surface:

$$\begin{aligned} F_\psi(\rho, \gamma) = \frac{K_a}{4}\Bigg\{&\sin^2\rho\cos^2\gamma\left[1 - \frac{1}{2(1 + 4D_R\tau)}\right] \\ &+ \cos^2\rho\sin^2\gamma\cos^2\gamma\left[1 + \frac{1}{2(1 + 4D_R\tau)}\right]\Bigg\} \\ &+ \frac{1}{4}(K_b\cos^2\psi + K_c\sin^2\psi) \\ &\cdot\Bigg\{(\sin^4\rho + \cos^4\rho)\sin^2\gamma\left[1 - \frac{1}{2(1 + 4D_R\tau)}\right] \\ &+ \sin^2\rho\cos^2\rho(\sin^4\gamma + 1)\left[1 + \frac{1}{2(1 + 4D_R\tau)}\right] \\ &- \frac{2\sin^2\rho\cos^2\rho\sin^2\gamma}{1 + 4D_R\tau}\Bigg\} + \frac{1}{4}(K_b\sin^2\psi + K_c\cos^2\psi) \\ &\cdot(\sin^4\rho + \cos^4\rho\sin^4\gamma + 2\sin^2\rho\cos^2\rho\sin^2\gamma) \\ &\cdot\left[1 + \frac{1}{2(1 + 4D_R\tau)}\right] \\ &- \frac{(K_c - K_b)}{2}\sin\psi\cos\psi(\sin^3\rho\cos\rho\cos^2\gamma \\ &+ \cos^3\rho\sin\rho\sin^2\gamma\cos^2\gamma)\left[1 + \frac{1}{2(1 + 4D_R\tau)}\right]. \end{aligned} \quad \text{(B11)}$$

Note that Eq. B11 has no $\alpha$ or $\beta$ dependence because the components $x_i$ of an absorption or emission dipole moment aligned parallel to the membrane plane are independent of the presence or absence of a net phospholipid tilt relative to the bilayer normal.

Image processing software was written by Jim DiGuiseppi and Barnaby Wray. Helpful discussions with James Casteel, Ken Jacobson, Brian Herman, and John Lemasters are gratefully acknowledged.

This work was carried out in the laboratory of Brian Herman and was supported by a fellowship from the University of North Carolina at Chapel Hill Curriculum in Toxicology (National Institutes of Health grant 5T32ES07126) to the author, and also by grants from the NIH (AG07218) and the Office of Naval Research (J-1433) to Brian Herman and John Lemasters.

*Received for publication 7 November 1989 and in final form 1 February 1990.*

## REFERENCES


Ameloot, M., H. Hendrickx, W. Herreman, H. Pottel, F. Van Cauwelaert, and W. van der Meer. 1984. Effect of orientational order on the decay of the fluorescence anisotropy in membrane suspensions. *Biophys. J.* 46:525–539.

Andrich, M. P., and J. M. Vanderkooi. 1976. Temperature dependence of 1,6-diphenyl-1,3,5-hexatriene fluorescence in phospholipid artificial membranes. *Biochemistry.* 15:1257–1261.

Axelrod, D. 1979. Carbocyanine dye orientation in red cell membrane studied by microscopic fluorescence polarization. *Biophys. J.* 26:557–574.

Axelrod, D. 1989. Fluorescence polarization microscopy. *In* Methods in Cell Biology. Vol. 30. D. L. Taylor and Y.-L. Wang, editors. Academic Press, Inc., San Diego, CA. 333–352.

Burghardt, T. P. 1984. Model-independent fluorescence polarization for measuring order in a biological assembly. *Biopolymers.* 23:2383–2406.

DiGuiseppi, J., R. Inman, A. Ishihara, K. Jacobson, and B. Herman. 1985. Applications of digitized fluorescence microscopy to problems in cell biology. *Biotechniques.* 3:394–403.

Engel, L. W., and F. G. Prendergast. 1981. Values for and significance of order parameters and "cone angles" of fluorophore rotation in lipid bilayers. *Biochemistry.* 20:7338–7345.

Florine-Casteel, K., and G. W. Feigenson. 1988. On the use of partition coefficients to characterize the distribution of fluorescent membrane probes between coexisting gel and fluid lipid phases: an analysis of the partition behavior of 1,6-diphenyl-1,3-5-hexatriene. *Biochim. Biophys. Acta.* 941:102–106.

Grant, C. W. M. 1983. Lateral phase separations and the cell membrane. *In* Membrane Fluidity in Biology. Vol. 2. R. C. Aloia, editor. Academic Press, New York. 131–150.

Jain, M. K. 1983. Nonrandom lateral organization in bilayers and biomembranes. *In* Membrane Fluidity in Biology. Vol. 1. R. C. Aloia, editor, Academic Press, New York. 1–37.

Kinoşita, K., Jr., S. Kawato, and A. Ikegami. 1977. A theory of fluorescence polarization decay in membranes. *Biophys. J.* 20:289–305.

Lemasters, J. J., J. DiGuiseppi, A-L. Nieminen, and B. Herman. 1987. Blebbing, free calcium, and mitochondrial membrane potential preceding cell death in hepatocytes. *Nature* (*Lond.*). 325:78–81.

Lentz, B. R. 1988. Membrane "fluidity" from fluorescence anisotropy measurements. *In* Spectroscopic Membrane Probes. Vol. I. L. M. Loew, editor. CRC Press, Inc., Boca Raton, FL. 13–41.

Lipari, G., and A. Szabo. 1980. Effect of librational motion of fluorescence depolarization and nuclear magnetic resonance relaxation in macromolecules and membranes. *Biophys. J.* 30:489–506.

Mabrey, S., and J. M. Sturtevant. 1976. Investigation of phase transitions of lipids and lipid mixtures by high sensitivity differential scanning calorimetry. *Proc. Natl. Acad. Sci. USA.* 73:3862–3866.

McFarland, B. G., and H. M. McConnell. 1971. Bent fatty acid chains in lecithin bilayers. *Proc. Natl. Acad. Sci. USA.* 68:1274–1278.

Mueller, P., T. F. Chien, and B. Rudy. 1983. Formation and properties of cell-size lipid bilayer vesicles. *Biophys. J.* 44:375–381.

Mulders, F., H. van Langen, G. van Ginkel, and Y. K. Levine. 1986. The static and dynamic behaviour of fluorescent probe molecules in lipid bilayers. *Biochim. Biophys. Acta.* 859:209–218.

Prendergast, F. G., R. P. Haugland, and P. J. Callahan. 1981. 1-[4-(Trimethylamino)phenyl]-6-phenylhexa-1,3,5-triene: synthesis, fluorescence properties, and use as a fluorescence probe of lipid bilayers. *Biochemistry.* 20:7333–7338.

Santaren, J. F., M. Rico, J. Guilleme, and A. Ribera. 1982. Thermal and $^{13}$C-NMR study of the dynamic structure of 1-palmitoyl-2-oleoyl-sn-glycero-3-phosphocholine and 1-oleoyl-2-palmitoyl-sn-glycero-3-phosphocholine in aqueous dispersions. *Biochim. Biophys. Acta.* 687:231–237.

Straume, M., and B. J. Litman. 1987. Equilibrium and dynamic structure of large, unilamellar, unsaturated acyl chain phosphatidylcholine vesicles. Higher order analysis of 1,6-diphenyl-1,3,5-hexatriene and 1-[4-(trimethylammonio)phenyl]-6-phenyl-1,3,5-hexatriene anisotropy decay. *Biochemistry.* 26:5113–5120.

Stubbs, C. D., T. Kouyama, K. Kinosita, Jr., and A. Ikegami. 1981. Effect of double bonds on the dynamic properties of the hydrocarbon region of lecithin bilayers. *Biochemistry.* 20:4257–4262.

Tardieu, A., V. Luzzati, and F. C. Reman. 1973. Structure and polymorphism of the hydrocarbon chains of lipids: a study of lecithin-water phases. *J. Mol. Biol.* 75:711–733.

Tsay, T-T., R. Inman, B. Herman, and K. Jacobson. 1990. Characterization of low light level cameras for digitized video microscopy. *J. of Microsc.* (*Oxf.*) In press.

van Langen, H., Y. K. Levine. M. Ameloot, and H. Pottel. 1987. Ambiguities in the interpretation of time-resolved fluorescence anisotropy measurements on lipid vesicle systems. *Chem. Phys. Lett.* 140:394–400.

von Sengbusch, G., and A. Thaer. 1973. Some aspects of instrumentation and methods as applied to fluorometry at the microscale. *In* Fluorescence Techniques in Cell Biology. A. A. Thaer and M. Sernetz, editors. Springer-Verlag, New York. 31–39.